Characteristics of Titan cell formation vary across clinical isolates of *Cryptococcus neoformans*

Xin Zhou[1], Hanna Zafar[1], Poppy Sephton-Clark[2], Sally H. Mohamed[3], Rebecca A. Drummond[3], Ivy M. Dambuza[4*], Elizabeth R. Ballou[1*]

[1]*Institute of Microbiology and Infection, School of Biosciences, University of Birmingham, Edgbaston, Birmingham, B15 2TT, UK*

[2]*Genome Sequencing and Analysis Program, Broad Institute of Harvard and Massachusetts Institute of Technology, Cambridge, 02142, Massachusetts, USA*

[3]*Institute of Microbiology and Infection, Institute of Immunology and Immunotherapy, University of Birmingham, Edgbaston, Birmingham, B15 2TT, UK*

[4]*Medical Research Council Centre for Medical Mycology, University of Exeter, Exeter, EX4 4QD, UK*

*To whom correspondence should be addressed:

Ivy M. Dambuza: i.m.dambuza@exeter.ac.uk

Elizabeth R. Ballou: e.r.ballou@bham.ac,uk

Funding

XZ is supported by a studentship from the Darwin Trust. HZ is supported by an NC3Rs PhD studentship (NC/R001472/1). PSC was funded by a BBSRC MIBTP PhD studentship. RAD and SHM are supported by the Academy of Medical Sciences (SBF004_1008) and the Medical Research Council (MR S024611_1). IMD is funded by the Wellcome Trust (102705 and 097377) and the MRC Centre for Medical Mycology (MR/N006364/1). ERB is supported by a Sir Henry Dale Fellowship jointly funded by the Wellcome Trust and the Royal Society (211241/Z/18/Z).

Importance

Many human fungal pathogens undergo morphological transitions to survive in the host environment. In response to host stimuli, the human fungal pathogen *Cryptococcus neoformans* exhibits an unusual yeast-to-titan morphological switch that contributes to disease development by altering immune polarization and introducing aneuploidy underlying host stress and drug resistance. Titans comprise a minority population and are defined by size, DNA content, and changes in cell wall and capsule structure using standard laboratory isolates. However, questions remain about the identification of this switch among clinical isolates. Here we demonstrate that population heterogeneity exists widely among *in vivo* mouse-passaged and *in vitro*-induced Cryptococcal clinical isolates, regardless of titanizing capacity. Upon encountering host environmental stimuli, aneuploid daughters are generated both by titanizing and non-titanizing isolates, resulting in populations with altered drug resistance. Studying population heterogeneity in the context of clinical isolates will improve understanding of the role of aneuploidy in disease outcomes.

Abstract

Upon encountering the host environment, fungal pathogens undergo morphogenic switches to mediate immune evasion and dissemination. The *Candida ablicans* yeast-to-hyphal switch and *Histoplasm capsulatum* mycelial-to-yeast switch both contribute to pathogenesis, and switch-deficient mutants show reduced virulence. In response to the host lung environment, the basidiomycete *Cryptococcus neoformans* exhibits an unusual yeast-to-titan transition thought to enhance pathogenicity by increasing fungal survival in the host lung and dissemination to the central nervous system. In a common laboratory strain (H99), titan cells affect virulence via increased cell size and ploidy, reduced phagocytosis, altered cell wall structure, and increased survival under host and drug stress. However, clinical and environmental isolates show a wide range in their capacity to switch, and the extent of this variation and implications for virulence remain unknown. Using new *in vitro* induction models, we are now able to generate titans that exhibit all the features of *in vivo*-generated titans. Here, we characterize key changes in clinical isolates after titanization, revealing that non-titanizing strains also show high population heterogeneity both *in vitro* and *in vivo*. In addition to reinforcing previously demonstrated *in vivo* phenotypes, we show that “non-titanizing” isolates differentially recruit immune cells, exhibit altered PAMP exposure over time, and can still generate aneuploidy *in vitro* and *in vivo* with implications for drug resistance in both the lung and the brain.

Introduction

Cryptococcus neoformans is worldwide opportunistic human fungal pathogen causing life-threatening pneumonia and meningitis in immunocompromised and immunocompetent individuals (1, 2). Cryptococcosis occurs when desiccated yeast or spores are inhaled, proliferate in the host lung and further disseminate into the central nervous system (2, 3). In response to the earliest interactions with host lung stimuli, *C. neoformans* cells undergo an unusual morphogenic switch, changing from small haploid yeast to large polyploid titan cells (4-9). While titan cells are defined as those cells larger than 10 μm in diameters, *in vivo* they can reach up 50 to 100 μm; typical yeast cells are around 5 μm (4, 5, 10). In addition to cell size, titan cells exhibit a thickened cell wall and maintain a characteristic single, large intracellular vacuole that occupies the majority of the intracellular space (5). At the same time, enlarged cell size is correlated with increased DNA content: Titan cells have high ploidy-often being tetraploid or octoploid-and they can produce diploid, aneuploid, or haploid daughters with normal cell sizes (4, 5, 11). More important, titan cells show altered virulence attributes: they have highly compacted polysaccharide capsule and altered Pathogen Associated Molecular Pattern (PAMP) exposure, including altered chitin and chitosan content in the cell wall (5, 12, 13). Titan cells are also less frequently phagocytosed, and more resistant to lung phagocyte killing and antimicrobial nitrosative and oxidative stress (4). Titanization is reported to be associated with altered host immune response and thought to enhance the virulence of *C. neoformans*(4, 5, 14)

In the past, one of the biggest challenges hampering further understanding of the molecular mechanisms driving titanization and their contribution to disease outcome was the lack of an *in vitro* titan cell induction protocol (10, 15-17). The process of titanization is triggered by environmental stimuli from the host lung, and our group and others have demonstrated that host-relevant stimuli are able to induce titan cells *in vitro* (9, 15-17). These *in vitro* generated titan cells exhibited similar features to *in vivo* induced titan cells, including: enlarged cell sizes, tightly compacted capsule, thicker cell wall, high ploidy and the presence of a single, large vacuole (9, 10). In our lab, the *in vitro* titan cell induction protocol is a two-step process: first *Cryptococcus* cells are incubated under nutrient starvation medium to mimic environmental conditions before entering into host, and then titan cells are induced with PBS+10%HI-FCS at low cell density (OD_{600}=0.001) (9, 15).

Previous work defining titan cells has focused on identifying genetic regulators *in vivo* and *in vitro* as well as characterizing environmental and host-derived stimuli (4, 5, 14,

18-20). However, the vast majority of this work has been done in the H99 laboratory strain. The extent of titanization in *C. neoformans* clinical isolates therefore remains unclear. Moreover, the relationship between the titanization capacity of a given strain and virulence remains poorly understood (21, 22). In fact, our initial screen of clinical and environmental *C. neoformans* isolates representing VNI, VNII and VNB clades revealed wide variation in the capacity of pathogenic strains to titanize (15). We classified them into three groups based upon their ability to produce titan cells: titanizing, non-titanizing and indeterminate, based on the definition of titans established by Zaragoza and Nielsen (10, 15)

In this study, we perform a careful phenotypic characterization of four representative clinical isolates that are genetic closely related while displaying a range of titanization capacities and *in vivo* disease outcomes. We found that, like titanizing strains, 'non-titanizing' strains also display population heterogeneity in both cell wall structure and DNA content after exposure to our *in vitro* induction protocol and after incubation in the murine lung, and that these phenotypic changes have consequences for the emergence of aneuploidy-driven drug resistance.

Results

In this study, we examine clinical isolates previously collected from the ACTA Lusaka Trial in Lusaka, Zambia (23, 24). We previously showed that Zambian clinical and environment strains collected by Vanhove et al. vary widely in their capacity to form titan cells, irrespective of originating niche or genotype (15). Here, we further characterize titanization in four strains- H99, Zc1, Zc8 and Zc12- selected based on their capacity to form titan cells *in vitro*. All four strains have been fully sequenced and genotyped and are genetically closely related (VNI). Using the size definition established by Nielsen and Zaragoza, Zc8 was previously classified as titanizing and Zc1 and Zc12 were previously classified as non-titanizing (Figure 1A) (10, 15). We have previously shown that Zc1 exhibits reduced virulence compared to H99, and that all four isolates produce melanin to comparable levels (15). When assessed for capacity to mate with KN99 MAT**a**, Zc1 and Zc12 were observed to form robust hyphae and sporulating basidia after 7 days, comparable with H99. Zc8, a MATα isolate, exhibited a profound defect in the formation of hyphae, with sporulating basidia rarely visible even after 3 months (Supplemental Figure S1A).

We assessed relative virulence of the four isolates using a wax moth larva model shown to be predictive of titan cell-mediated virulence in mice (25, 26). When pre-grown in YPD, the

four strains produced significantly different survival curves (n=10, Gehan-Breslow-Wilcoxon test, p=0.00070) (Supplemental Figure S1B). However, despite differences in titanization capacity, this difference disappeared when strains were pre-grown in titan inducing conditions (Supplemental Figure S1B).

In vitro titan inducing conditions trigger a range of cell size and DNA content changes across four clinical isolates

We set out to fully characterize titanization in the four strains. The most striking feature of titan cells is their large cell size, and a number of reports have attempted to quantify titan, titan-like, or "giant" cells *in vitro* across clinical isolates using either 10 μm or 15 μm size thresholds and microscopic examination of a small number of cells (21, 27). We therefore first examined cell size distribution across the four clinical isolates under *in vitro* titanizing conditions. Upon *in vitro* induction, H99 and Zc8 produce highly heterogeneous populations comprising titans (>10 μm), titan daughters (titanides, >1 μm and <3 μm oval cells) and yeasts, while Zc1 and Zc12 populations are more uniform (Figure 1B). When measured by microscopic visualization, cells >10 μm account for about 15% of the H99 total population, but only approximately 2% in Zc8. Moreover, induced non-titan Zc8 cells (<10 μm) are smaller on average than non-titan H99 cells (3.80 μm ± 0.10 vs 7.15 μm ± 0.14 SEM, $p<0.0001$, n>200), and are smaller on average than Zc1 or Zc12 induced cells (4.44 μm ± 0.05, 4.57 μm ± 0.06 SEM, respectively, $p<0.0001$, n>200).

Given the low frequency of titans detected in induced Zc8 cultures, which can easily be missed when relying on cell counts with small numbers, we assessed cell size spread across the population of a large number of cells by flow cytometry. Using this approach, we observed population structure characteristic of typical and titan populations for both H99 and Zc8, with a minority sub-population of cells distinguishable as a clear shoulder by forward scatter (FSC, a proxy for cell size) (Figure 1Ci, n>8000). However, the median FSC of cells comprising that shoulder was lower in the Zc8 population than in the H99 population (Figure 1Cii). In addition, a minority of Zc1 cells, but not Zc12 cells, exceeded the threshold for H99 titan cells (Figure 1Cii), suggesting the presence of cells >10 μm in the Zc1 isolate not detected by other methods.

Titan cells are defined as those cells >10 μm and with increased ploidy (>2C)(10), where size increase is proportional to the increase in DNA content, as has been observed for other fungal species (4, 5, 28-30). We therefore assessed cell ploidy across the induced populations

by flow cytometry. Cells were methanol fixed and incubated with DAPI (4',6-Diamidino-2-Phenylindole, Dihydrochloride) to quantitatively stain DNA in all induced populations, and cell ploidy was assessed by comparison to YPD-grown matched parental isolates using established protocols, including gating strategies for single cells (Supplemental Figure S1Ci) (15). The majority of induced H99 cells had DAPI staining consistent with 1C content, and the overall population showed the characteristic stepwise increase in DAPI intensity indicative of polyploidy, with peaks indicating the presence of titans with DNA content up to 16C after 24 hours (Figure 1D).

We applied a similar analysis to induced Zc8 cells. Interestingly, the overall DNA staining intensity of induced Zc8 cells was lower than that of Zc1, Zc12, or H99 induced cells, consistent with their reduced cell size. Examination of the DNA content of YPD-grown Zc8 cells revealed an overall reduction in 1C and 2C peak MFI relative to H99 YPD-grown cells (Supplemental Figure S1Cii), and this was confirmed by whole genome sequencing (data not shown). Despite this overall reduction, a majority of induced Zc8 cells were 1C and a similar stepwise population of polyploid cells with a long tail to the right was apparent (Figure 1D). Gating identified ~3% of cells with DNA content ≥4C, and these cells were similar in size to H99 4C cells (Supplemental Figure S1Ciii), consistent with an overall size increase >10 μm.

When we examined DNA content in Zc1 and Zc12 induced populations, in which no cells >10 μm had been observed, we did identify rare polyploid cells. Unlike H99, the majority of cells in these populations had DAPI staining consistent with 2C DNA content, or G2 arrest, typical of *C. neoformans* incubated in minimal medium or low aeration (31, 32). For Zc1, a 4C population comprising <2% of the total population was identified (Figure1D). Again, these cells were similar in size to H99 4C cells, confirming the presence of rare titan cells in the Zc1 culture (Supplemental Figure S1Ciii). However, for Zc12, cells with DNA content consistent with >4C were smaller than either H99 4C or 2C cells (Supplemental Figure S1Ciii), consistent with these cells being aneuploid but not true titan cells.

Finally, all four induced populations also contained cells with apparent “sub-1C” DNA content, represented as stepwise peaks to the left (Figure 1D; H99:6.4%; Zc1: 6.7%; Zc8; 25.6%; Zc12:2.7%). We speculated that these peaks might represent titanide cells: oval, nucleate cells of 2-3 μm in diameter which we previously demonstrated are also associated with *in vitro* induced titan cells (15). Similar peaks have been observed during cell cycle analysis of *Saccharomyces cerevisiae* and are representative of G0 or quiescent cells (33, 34). Ashton et al. have recently suggested that the existence of robust quiescent cells such as

spores might contribute to the broad ecological distribution of specific sub-clades, however the rarity of MAT**a** *C. neoformans* isolates in the environment suggests an alternate origin for these cells (35, 36). We speculated that titanides might share similarity to *C. neoformans* spores produced by mating. To test this hypothesis, H99 matα cells were crossed with KN99 MAT**a** cells, incubated for 2 weeks to ensure robust sporulation. The mating front, representing hyphae, basidia, spores, and some contaminating yeast, was excised, and filtered through an 11 μm filter to exclude large particles. The resulting population was fixed, stained and analysed by flow cytometry alongside yeast-phase cells to identify 1C and 2C gates and a "sub-1C" background of <2.5%, set as a threshold for false positives. This analysis revealed a "sub-1C" peak to be a major population in robust mating reactions (H99: 37%; Zc1:34%; Zc12:53%) and a minor population (10%) in the Zc8 mating front, in which basidia were rarely observed (Figure 1E, Supplemental Figure S1A). Direct comparison to titan-induced H99 cultures revealed a similar "sub-1C" peak (8%) consistent with titanides and suggestive that this population represents quiescent G0 cells.

Therefore, based on *in vitro* phenotyping by flow cytometry for both cell size and DNA content, we would predict that H99 and Zc8 isolates will form titans *in vivo*, with the overall size of Zc8 populations smaller than that of H99, that a minority of Zc1 titan cells might be detected, and that Zc12 would fail to produce titans *in vivo*.

***In vivo* titan inducing conditions match *in vitro* predictions**

We next assessed all four strains in a murine inhalation model of cryptococcosis, the gold standard for determining titan capacity. Mice were infected intra-nasally with $5x10^5$ cells pre-cultured in sabouroud dextrose medium according to standard infection protocols, and brain and lung fungal burdens were measured after 10 days. Work using H99-derived mutants has demonstrated a role for titan cells in survival and proliferation in the pulmonary environment as early as day 7 (14). When fungal cells from lung homogenates were analysed microscopically for titanization *in vivo*, similar size distributions were observed as seen *in vitro* (Figure 2A). Specifically, robust titanization was observed for both H99 and Zc8 (65% and 68% of cells recovered from the lung, respectively, >10 μm), with Zc8 population covering a significantly smaller size range than H99 (Kolmogorov-Smirnov test for cumulative distribution, p=0.0001). A minority (8%) of Zc1 cells were >10 μm. No Zc12 cells >10 μm was observed. Similar to *in vitro* induced Zc1 and Zc12 cells, the *in vivo* populations as a whole were more uniform in overall structure. In our hands, the four clinical

strains showed similar fungal burdens in the lungs on day 10 (Figure 2B, $p>0.05$) as assessed by CFUs, demonstrating similar capacities to proliferate early during infection. Consistent with this, brain CFUS were comparably low, with Zc1 dissemination slightly higher than the others (Figure 2C; $p<0.01$). Despite similar disease progression at this early time point, we observed differences in interaction with host immune cells: Zc1 elicited significantly more neutrophil recruitment compared to H99 and Zc8 (Figure 2D; $p=0.003$, 0.0011, respectively) while H99 elicited increased alveolar macrophage recruitment compared to Zc8 and Zc12 (Figure 2E; $p=0.028$, 0.043). There were no differences in the recruitment of interstitial macrophages across the four groups (Supplemental Figure 2).

Clinical isolates show different capacities to disseminate and produce aneuploid colonies

Next, we examined the ploidy of individual colonies originating from lung and brain CFUs (Figure 3A, Supplemental Figure S2A, $n=30$ for lung CFUs, $n\geq10$ for brain CFUs, across 3 mice per isolate). Colonies were assessed within 72 hours of recovery from mice, at the point when a small colony was just visible on YPD agar (~36 generations), a measure of stable aneuploidy in the absence of environmental stress. Figure 3 shows ploidy of individual colonies relative to the median ploidy of all colonies from that particular lineage. There was no significant difference in relative ploidy between colonies from lung vs. brain isolates for any of the isolates. We observed that ploidy of H99 and Zc8 colonies varied widely, while Zc1 colonies were more uniform ($p=0.02$ compared to H99). This is consistent with a high degree of titanization driving aneuploidy in H99 and Zc8 infections, and relatively low titanization in the Zc1 isolate. However, we observed widespread instances of aneuploidy in Zc12 CFUs, despite finding no evidence of true titanization in this strain either *in vitro* or *in vivo*.

Aneuploidy is associated with increased resistance to fluconazole, which continues to be used as a frontline antifungal in resource limited settings. Fluconazole resistance in *C. neoformans* is linked to aneuploidy of chromosomes 1, 4, 6, and 10 due to the presence of genes on these chromosomes that directly enable fluconazole resistance, however the contribution of titanization to resistance remains unclear (37). We therefore assessed the impact of altered ploidy on drug resistance of individual colonies isolated from the lungs and brains of infected mice (Figure 3B). Relative to parent isolates, we observed a wide range in capacity to proliferate in the presence of fluconazole. The distribution of resistance for Zc12-derived colonies was significantly limited compared to those of H99, Zc8, or Zc1 ($p\leq0.0002$). For H99, both fluconazole resistant and sensitive colonies were identified. For Zc8, colonies

with increased resistance to fluconazole tended to have increased ploidy, but a colony with reduced overall ploidy and increased drug resistance was also observed. For Zc1 aneuploid colonies were uniformly more sensitive to the drug. Within individual lineages there was no correlation between increased or decreased ploidy and degree of fluconazole resistance (R^2<0.3 in all cases). This is consistent with aneuploidy in these isolates being random rather than specific amplification of chromosomes involved in fluconazole resistance occurring prior to drug exposure.

The presence of Titan cells leads to decreased phagocytosis

We next investigated the interaction of the strains with immune cells *in vitro.* During initial cryptococcal infection in the host lung, resident alveolar macrophages are amongst the first immune cells to encounter *Cryptococcus*, and the outcome of this interaction is predicted to determine the course of infection (38, 39). To model the impact of titanization on disease development, we first studied the *in vitro* interactions between these four strains and murine J774.1A macrophage-like cells, a commonly used proxy for *Cryptoccocus*-macrophage interactions (20, 40, 41). Each of the four clinical isolates was incubated in titan-inducing conditions for 24 hours and then co-incubated with phagocytes for 2 hours. To differentiate engulfed and un-engulfed cells, calcofluor white was added to the medium prior to fixation and imaging. We observed significant variation in the percent of macrophages containing at least one internalized *C. neoformans* cell across the four isolates (Figure 4A). For titan-induced cells, H99 showed the lowest macrophage infection rate and was significantly reduced compared to the other 3 strains (Figure 4A) (compared to H99: Zc1, p=0.0063; Zc8, p=0.0131; Zc12, p=0.0164). As shown in Figure 4B, for both H99 and Zc8, it appeared that engulfed cells were typical cells (titanides and yeasts) rather than titan cells. Furthermore, staining with the capsule-specific antibody 18B7 revealed that during J774-titan co-incubation, H99 titan cells physically associated with macrophages but were not engulfed (Figure 4C). We therefore asked whether the reduced uptake of H99 cells overall relative to Zc8 (Figure 4A) might be a consequence of the higher proportion of titan cells in this population. To measure titan-induced H99 uptake in the presence and absence of the titan population, filtered titan (>10 μm) cells or typical (<10 μm) cells were used to infect macrophages separately. When only titan cells were present, the average macrophage infection was 21.6% ± 5.5 (SEM), while for typical H99 cells the rate was 82.2% ± 1.6 (SEM) (Figure 4D, p=0.0002, n=500), similar to uptake of the total populations for the three Zc strains. These results are consistent with previous studies *in vivo* showing that titan cells

are more resistant to phagocytosis and with the observation that these cells exert a protective effect on the uptake of smaller cells (4, 14)

Modeling fungal-phagocyte interaction *in vitro* reveals strain specific phenotypes

Typical cells make up the majority of cryptococcal cells *in vitro* and *in vivo.* Although these can be recognized and engulfed, most are able to survive within or escape from phagocytes via lytic or non-lytic mechanisms (42-44). To better understand the impact of titan and typical cells on disease development, we analyzed the infection process of all four strains following titan induction. Mixed cultures of titanized cells were co-incubated with macrophages *in vitro* and observed via time-lapse imaging for 18h. Intracellular Proliferation Rate (IPR), frequency of vomocytosis (vomo %), and frequency of macrophage death (Mϕ death %) were measured. No significant difference in IPR was observed for the four strains, indicating that they maintain similar intracellular growth rates (Figure 4E). Zc8 induced the highest frequency of vomocytosis, although it was not statistically significantly different ($p=0.05$ vs. Zc12) (Figure 4F), but did induce significantly more macrophage death ($p<0.001$) (Figure 4G; $n=400$). This suggests that there is no correlation between titanization capacity and vomocytosis or macrophage death.

Finally, we assessed the resistance of the four isolates to physiologically relevant concentrations of ROS stress. As shown in Figure 4H, while there was no difference in sensitivity prior to induction, after 18hrs H99 and Zc8 induced isolates were more sensitive to 0.5 μm H_2O_2 compared to Zc1 and Zc12.

Titan cells enhance the production of TNF

Titan cells have previously been reported to enhance the production of TNF, a marker of M1 and T_H1 polarization required for successful *Cryptococcus* infection control and involved in ROS generation (45, 46). We quantified the levels of TNF produced following stimulation of murine J774 macrophage-like cells or human blood derived monocytes with the four clinicals isolates following culture in normal or titan inducing conditions. As shown in Figure 5A, after 24 hrs there was increased accumulation of TNF for macrophages infected with either induced H99 ($p<0.0001$) or Zc8 ($p=0.01$) cells compared to their un-induced controls. In particular, H99 titanized cells showed an almost 10-fold increase compared with Zc1 and Zc12 strains pre-cultured under titanizing conditions (Figure 5A). However, induced Zc8 cells also elicited increased TNF compared to induced Zc1 ($p=0.004$) or Zc12 ($p=0.0002$). This increase can primarily be explained by the presence of titan cells: when macrophages

were infected with filtered H99 titan cells, there was significantly higher accumulation of TNF compared to a mixed infection ($p<0.0001$) or to pre-induced typical cells alone ($p<0.0001$) (Figure 5B). Circulating blood monocytes are increasingly recognized as essential players in innate and adaptive immune responses against a wide range of microbes (47-49). Human monocytes derive from progenitors in the bone marrow and can supply tissues with macrophages and dendritic cell (DC) precursors that contribute to antimicrobial defense (50-52) However, Heung et al. recently showed that during infection, *C. neoformans* can influence inflammatory monocyte polarization to an alternatively activated M2-like profile which are poor producers of ROS and are detrimental to the host response (49). To investigate the impact of titan cells on monocyte activation, we TNF production by human blood-derived monocytes infected with each of the 4 strains pre-grown under titanizing conditions (Figure 5C). As early as 4hrs following incubation, H99 titanized cells showed higher production of TNF compared with the other three strains (Compared with T-H99: all $p<0.0001$) which substantially increased by 24hrs of culture (Figure 5C; Compared with T-H99: all $p<0.0001$). As shown in Figure 5C, monocytes infected with H99 titanized cells showed higher production of TNFα compared with the other three strains (Compared with T-H99: all $p<0.0001$). Together, these data demonstrate that *in vitro* titan cells are immunologically distinct from typical cells and their capacity to robustly modulate a pleiotropic cytokine like TNF suggest that titan cells may influence disease outcome in a heterogeneous infection.

Titan induction can cause differential increases in capsule size and capsule compositions

The *C. neoformans* cell wall is covered by a protective capsule, which not only impairs phagocytosis by macrophages, but also mask PAMPs from being engaged by host PRRs (53). Moreover, H99 titan cells have been reported to have altered capsule compared to yeast (5, 54). We have previously demonstrated that Crp127 is an anti-capsule monoclonal IgM (Immunoglobulin M) antibody associated with O-mannosylation, to capsular polysaccharide and that its localization is dynamic throughout titan development (54). We therefore assessed the capsule of Zc isolates after titan induction. Induced cells were stained with both India ink to reveal overall capsule size and Crp127 IgM antibody to reveal localization of the Crp127 epitope (Figure 6A,B) (54). All the isolates expressed robust capsule and were reactive to Crp127 IgM, consistent with our previous reports (Figure 6A). Binding was found to be heterogeneous across the population, with both stained and unstained cells observed within all induced populations, and different binding patterns across cells in a given population

(Figure 6A). Analysis of capsule to cell body ratio for each of the populations revealed that Zc12 cells display reduced capsule compared to the other isolates ($p<0.0001$, $n>100$) (Figure 6B).

Flow cytometric analysis of Crp127 binding revealed a high degree of heterogeneity in induced populations (Figure 6C,D). For H99 and Zc12, more than 50% of the total population was positive for IgM binding, while for Zc1 less than half of the population was positive. Only 5% of Zc8 cells were positive for IgM binding, and this correlated with the largest cells (Figure 6Dii). Moreover, the distribution of Median Fluorescence Intensity differed across populations: For H99 and Zc1 populations, multiple different populations of capsule staining intensity were present in induced cultures, with H99 staining more brightly overall. In contrast, Zc8 exhibited more uniformly low staining overall, and Zc12 was more uniformly high. These together, these data suggest that even in the absence of true titan cells, inducing conditions significantly impact capsule structure, with a high potential for altered capsular organization across genetically related clinical isolates.

Induced cells exhibit changes in PAMP exposure

Examination of *C. neoformans* cells recovered from mouse lung have demonstrated that titan and typical cells have different cell wall composition, with an increase in chitin and mannose (including mannan, mannoproteins, and capsular mannans) observed in cells > 10 μm (12, 13). We therefore asked whether similar differences could be observed in *in vitro* induced cells. Chitin (Calcofluor white, CFW), chitosan (EosinY), and cell wall mannan (ConA) were measured following exposure to inducing conditions for 24 hours. Representative images for all four strains in both YNB and following induction can be seen in Figure 7A. FACS analysis revealed an overall decrease in PAMP exposure following titan induction (Figure 7Bi, H99 representative plot), likely as a result of capsule expression masking surface exposure. However, induced populations were not uniform in the extent of their cell wall organization following induction (Figure 7Bii). Gating on positively staining cells only, we observed that chitin, mannan, and chitosan staining were correlated with cell size, with larger cells staining more intensely than smaller cells, the majority of which were below the threshold of detection (Figure 6bii). Moreover, distinct high chitin populations were apparent in H99, Zc1, and Zc8 cultures (Supplemental Figure 3A). Quantitative analysis by flow cytometry using the same approach to identify titan cells as taken in Figure 1C again revealed a sub-population of large cells in induced H99, Zc8, and Zc1 cultures

(Supplemental Figure 3A). Similar to *in vivo*-derived H99 titan cells, *in vitro*-induced H99, Zc1 and Zc8 cells displayed a distinct CFW-high population that correlated with the largest cells (Figure 7B, Supplemental Figure 3B). However, the largest Zc12 cells also exhibited the highest overall chitin staining (Figure 7B, Supplemental Figure 3B). Large cell populations for all isolates had comparable chitosan and cell wall mannan staining to typical cells (Supplemental Figure 3B). Moreover, in long-term induced cultures (72 h), overall heterogeneity was more apparent, with distinct high and low chitin peaks present in both Zc1 and Zc12 populations (Figure 7C). These data suggest that after exposure to titan inducing conditions, both titanizing and non-titanizing isolates are heterogeneous with regard to PAMP exposure.

Discussion

The Yeast-to-Titan transition is an important morphogenetic switch for *C. neoformans* that can affect drug resistance and host immune responses, contributing to poor disease outcome (4, 5, 14, 19). A pressing question has been the capacity of clinical and environmental isolates to form titan cells, with authors applying *in vivo* titan definitions, primarily cell size, to cells grown in a variety of *in vitro* conditions (21, 22). With the development of robust *in vitro* titan cell induction models, we are now able to reproduce titan cells *in vitro* using host-relevant environment signals such as serum and CO_2 (15-17). Here, we expand upon the *in vivo* definition of titan cells to encompass the wide phenotypic diversity observed during *in vitro* induction of three clinical isolates from the ACTA Lusaka Trial in Lusaka, Zambia (23, 24). By analyzing cell size, ploidy, cell wall organization and capsule properties, as well as by studying their interactions with murine macrophages and human monocytes we begin to reveal complexity surrounding the impact of induced cells on different immune events including phagocytosis, vomocytosis and activation of the immune response.

Defining titanization in clinical isolates

Building on our previous findings, we used 4 clinical strains from the same genetic clade (VNI) which we had previously identified as having different capacities to produce titan cells (15). H99, Zc1, Zc8 and Zc12 demonstrated significant population heterogeneity after exposure to inducing conditions, regardless of titan status. Relative to Zc8, H99 is strongly titanizing *in vitro* when the *in vivo* definition (> 10 μm) is applied, but that Zc8-induced cells

exhibit overall population structure consistent with titanization, including polyploidy (>4C), a relative increase in cell size, and overall changes in PAMP organization. We outline a gating strategy that will enable others to identify polyploid cells >10 μm in clinical isolates relative to H99 following *in vitro* culture, and will also enable cytometric identification of polyploid cells that fail to cross the 10 μm threshold. We additionally note that researchers can readily identify titan cells through visual inspection of liquid cultures in tissue culture plates using bright-field microscopy, with titans being those large cells with a single vacuole and an intensely dark cell wall apparent in H99, Zc8, and Zc1 cultures (Figure 1A).

Population heterogeneity appears to be a general feature of titanizing isolates. Here we observed that both titanizing strains H99 and Zc8 are highly heterogeneous after induction, with three sub-populations that maintain distinct cell sizes and DNA contents. Moreover, titan cells from both strains exhibit changes in PAMP exposure and capsule size and composition, features important for the virulence of *C. neoformans*. Additionally, non-titanizing induced strains also show population heterogeneity as measured by DNA content and cell wall structure, despite a lack of true titan cells. Moreover, induced but not un-induced cells from all isolates showed similar infection outcome when using the galleria model and we found no differences in capacity to control early lung fungal burdens during a mouse model of cryptococcosis. Our data therefore demonstrate that both non-titanizing and titanizing isolates respond to host environment signals and these changes will have implications for drug resistance and host cell interactions. Future studies will investigate long term immune responses including investigation of T cell polarization mediated by the different clinical isolates.

Impact of titanization on drug resistance

Cryptococcus neoformans displays fluconazole hetero-resistance: transient resistance in a subpopulation of cells mediated by aneuploidy of chromosomes that carry genes involved in fluconazole detoxification, and this impacts on disease outcomes (55-58). Gerstein et al. previously demonstrated that *in vivo*-derived titans provide daughters with a survival advantage compared to *in vivo*-derived typical cells. Titan-derived colonies are resistant to fluconazole via aneuploidy of chromosomes 1, 4, 10, 11, and/or 12 when propagated in the presence of fluconazole, suggesting that titanization drives fluconazole resistance *in vivo* (11, 37). Our data support these findings, with overall increases in population diversity in titanizing strains compared to non-titanizing strains following passage through mice (Figure

3A). However, we observed no specific correlation between increased ploidy and increased fluconazole resistance (Figure 3B). This is consistent with *in vivo*-induced aneuploidy being random with regard to particular chromosomes, rather than specific increase of chromosomes involved in fluconazole resistance. Semighini et al. previously demonstrated, using comparative genome hybridization arrays in H99-derived strains, that passage through mice in the absence of drug stress results in large scale genome alterations, including aneuploidy, insertions, and deletions (59). Consistent with this, we also observed large scale reductions in genome content relative to parent isolates. We add to these previous reports by showing that high titanizing H99 and Zc8, low-titanizing Zc1 and non-titanizing Zc12 isolates all yield aneuploid daughters to some degree when passaged through mice. We hypothesize that, in addition to strongly inducing titanization, passage through mice itself is sufficient to induce aneuploidy and exerts a selective pressure, as has been observed for *C. albicans* (60). Consistent with this, we previously reported that daughter cell colonies derived from *in vitro*-induced titan cells are mostly diploid, in conflict with reports from Gerstein et al. that colonies derived from *in vivo*-derived titan cells are haploid or aneuploid (11, 15)). This suggests that daughter cells derived from the two conditions may differ in their tolerance to aneuploidy or capacity for genome maintenance. Fluconazole exposure, oxidative stress, and high temperature drive *in vivo C. albicans* aneuploidy, including whole ploidy reduction (diploidy to haploidy), individual chromosome aneuploidy (Chr 5), and segmental aneuploidy, and the same is likely true for *C. neoformans* even in the absence of titanization (60-63).

Finally, ability to induce titan cells in simple conditions such as nutrient starvation followed by exposure to bacterial cell wall, conditions likely to be encountered by *Cryptococcus* in the environment, make it highly plausible that titan cells may form in the environment and are not just limited to patient lungs. This raises the hypothesis that "quiescent" cells proposed to drive population expansion in environmental isolates may be derived from titan cells (35). In fact, analysis of induced populations revealed "sub-1C" cells with similarities to spores generated through heterothallic mating (Figure 3C). Future work will examine the impact of environmental triggers on *C. neoformans* population heterogeneity and morphogenesis.

Influence of titanization on immune responses *in vitro*

After induction, H99 triggers higher production of TNF by mouse macrophages and human monocytes, innate cells important in restraining *C. neoformans.* This may indicate that titan

cells can activate host T_H1 immune response, diverging from reports that titan cells are associated with induction of a non-protective T_H2 response in mice (14, 64). Moreover, our data suggest that early titanizing cultures, at time points when titan mothers first become identifiable, are particularly vulnerable to M1-type ROS-mediated killing, while Gerstein et al. demonstrated that *in vivo*-derived titan cells can be more resistant to ROS stress, likely a result of their thickened cell wall (11). While the fungal cell wall PAMPs β-glucan and mannan have been demonstrated to trigger pro-inflammatory immune response via C-type lectin receptors, the *C. neoformans* capsule masks these PAMPs from the host, and the major ligand for *C. neoformans* recognition remains unclear (65). The dynamic nature of the titan cell wall, particularly chitin, and capsule relative to yeast suggest a complex strategy for host evasion (12, 66). We further demonstrate here that the penetrance of titanization within a population can impact the strength of the host response: purified H99 titans are potent TNF inducers, while mixed cultures are less stimulatory. The clinical isolate Zc8 can produce titan cells, however these comprise only 2% of the total population *in vitro*, and reach only around 11μm in cell body diameter. These distinct features of Zc8 may be the reason that *in vitro*-induced Zc8 cultures neither increased TNFα nor decreased phagocytosis. In addition, Zc8 co-cultures exhibited the highest vomocytosis and macrophage lysis rates, suggesting these features occur independent of the presence of large cells. Finally, both H99 and Zc8 *in vivo* produced high proportions of titan cells, suggesting a capacity to modulate or further activate titanization in the host lung. Together, our data demonstrate significant population heterogeneity, both within induced cultures over time and across closely related clinical isolates, demanding further investigation.

Acknowledgements

We thank the doctors, patients, and their families involved in the ATCA Lusaka trial, without whom this research would not have been possible. We thank the staff of the University of Birmingham BMSU for their assistance. 18B7 anticapsule antibody was a generous gift from Arturo Casadevall.

Materials and methods

Strains, media and growth conditions: All *C. neoformans* strains used in this study are listed in Table 1.

Strains	lineages	Clades	Source
H99	VNI	Clinical isolate	North Carolina
Zc1	VNI	Clinical isolate	Zambia
Zc8	VNI	Clinical isolate	Zambia
Zc12	VNI	Clinical isolate	Zambia

Strains were cultured routinely on YPD (1% yeast extract, 2% bacto-peptone, 2% glucose, 2% bacto-agar) plates stored at 4°C. For mating reactions, cells were mixed from YPD plates with KN99a directly on Murashige Skoog agar (M5519 Sigma-Aldrich) and incubated in the dark at room temperature for at least 2 weeks. Titan cell *in vitro* induction was performed as described in (15). Briefly, cells were pre-cultured at 37°C, 150rpm, in 10ml YNB without amino acids (Sigma-Aldrich) in which 2% of glucose was added according to manufacturer's protocol. After 24 hr, cells were normalized to OD_{600}=0.001 in 1×PBS (phosphate-buffered saline) with 10% of Heat inactivated Fetal Bovine Serum (HI-FBS) (Sigma-Aldrich F9665) and incubated at 37°C, 5%CO_2 for 24 hrs unless otherwise indicated.

***Galleria mellonella* infection model:** *G. mellonella* were purchased from LiveFoods, Ltd (UK) and used within 3 days of arrival. Worms were maintained at 16deg C until use, and only worms lacking melanization were included in the experiment. Worms were allocated randomly to each treatment group (10 per group), with the average weight of worms across treatment groups maintained within 0.002 g. Cryptococcus strains were incubated overnight in YPD (5% yeast extract, 10% bactopeptone, 2% D-glucose) at 150 rpm, 30 deg C. Cells were washed in sterile PBS, and then normalized to 5x 10^6/ml. Strains were randomly allocated to the different groups. Worms were injected into the back left pro-leg with 20 ul innoculum. Worms were maintained in the dark at 30 deg and observed for 10 days for survival, with blinding for the identities of the different treatment groups. Survival was analyzed by Kaplan-Meyer survival curve and significance was assessed by Log rank (Mantel-Cox) test.

Murine infection model: Female C57BL/6 mice were used at 8-10 weeks of age and were maintained in individually-ventilated cages under specific pathogen-free conditions at the Biomedical Research facility at the University of Birmingham (Birmingham, UK). Animals were provided with food and water *ad libitum.* All experimentation conformed to the terms

and conditions of United Kingdom Home Office license for research on animals (PPL/PBE275C33) and the University of Birmingham ethical committee.

Cryptococcosis Infection Model: Yeast was grown in SabDex broth(Sigma-Aldrich), grown at 30°C with shaking for 18-24 hours. Yeast cells were washed in PBS, counted, and delivered to mice intranasally while under isofluorane anaesthesia. Animals were infected with $2x10^5$ CFU. For analysis of lung and brain fungal burdens, animals were euthanized and organs weighed, homogenized in PBS, and serially diluted before plating onto YPD agar supplemented with Penicillin/Streptomycin (Invitrogen). Colonies were counted after incubation at 37°C for 48 hours.

Preparation of Lungs for FACS: Lungs were removed aseptically from euthanized animals, finely minced with a scalpel, and digested in digest buffer (RPMI supplemented with 10% FBS, 1% penicillin/streptomycin [Invitrogen], 1mg/mL collagenase D [Sigma], 1mg/mL dispase [Sigma], 40 μg/mL DNAse [Roche]) at 37°C for 30 minutes. Digested lungs were smashed through a 70μM filter, washed and red blood cells lysed on ice using BD PharmLyse solution. Lung-isolated cells were washed in PBS/2mM EDTA, and then stained with fluorophore-conjugated antibodies in the presence of anti-CD16/32 and 0.5% BSA for 30 minutes on ice. Samples were washed in PBS/0.5% BSA/0.01% sodium azide and acquired using the BD Fortessa instrument equipped with BD FACS Diva software (BD Biosciences). FlowJo (TreeStar) was used for the final analysis. Anti-mouse antibodies used in this study were: CD45 (30-F11), Ly6G (1A8), Ly6C (HK1.4), SiglecF (S17007L), all from Biolegend, and CD11b (M1/70), F4/80 (REA126), MHC Class II (REA813), all from Miltenyi Biotec.

J774.1 cell culture: For most *in vitro* infection assays, we used the J774.1 murine macrophage cell line. Cells were routinely passaged in Dulbecco's modifies Eagle medium (DMEM+) culture media with serum (DMEM, low glucose, from Sigma-Aldrich; 10% HI-FBS; 1% penicillin-streptomycin solution from Sigma-Aldrich; 1% 200mM L-glutamine from Sigma-Aldrich). All assays were performed with cells in passages 4 to 10.

Human primary monocytes isolation and culture: All human tissue work was performed as approved by the University of Birmingham Ethics Committee under reference ERN_15-

0804b. On day of draw, 25-30 ml of blood was withdrawn from anonymized healthy volunteers by venepuncture and was directly used for monocytes isolation with double layer percoll. Before adding the blood, two of different densities of percoll were layered in the universal tubes with 6 ml of 1.079 on the top and 6 ml of 1.089 at the bottom. After 6 ml of whole blood was layered over dual gradient, the universal tubes were centrifuged at 150g for 8mins, followed by 10mins at 129g without acceleration or breaks. The white disc of peripheral blood mononuclear cells (PBMCs) was removed from the top and mixed with red blood cell lysis buffer to clear away red blood cells. After centrifuge for 6 mins at 400g, PBMCs were washed twice in cold 1×PBS (centrifuged at 1000 g for 6 mins in between), resuspended in warm RPMI 1640 with 5% HI-AB serum, counted, and then plate onto 12 well plate at 1×10^6 cells per well. The covered plate was incubated at 37°C, 5%CO_2 overnight, after which non-adhere cells were removed by washing with fresh RPMI.

***In vitro* phagocytosis assays:** The intracellular proliferation assay was performed as previously described (61). 24h before infection, 1×10^5macrophages J774 were seed into 12-well plastic plates (Greiner) in 1 ml DMEM culture media with serum (DMEM+) and activated with 10 U/ml IFNγ. Before infection, *C. neoformans* cells were collected from titanization culture and washed three times with sterile 1×PBS. After normalising to 1×10^6 cells/ml in 300 μl DMEM+, cells were opsonized with 10μg/ml anticapsular 18B7 antibody by incubating at 37°C for 30min (62). Then opsonized *C. neoformans* cells were added into activated J774.1 macrophages to give a multiplicity of infection (MOI) ratio of 10:1. After 2 hr (time point 0), infected wells were washed at least three time with pre-warm 1×PBS until all un-engulfed *C. neoformans* cells were removed from the wells.
Human monocytes were infected with opsonized cells for 4h without IFNγ activation, and at this point all supernatants were collected for cytokine qualification. 4h post-infection, monocytes were divided into two groups: with or without IFNγ (10 U/ml) activation and then infection continued for another 20h. Total 24h later, all supernatants were collected again with LPS (100ng/ml) as a positive control added at the same time as fungal cells and uninfected as negative control.

Macrophage infection rates: At time point 0, attached *C. neoformans* cells and macrophages were stained with Calcoflour white (CFW, 10 μg/ml) and Lyso-Tracker Red (ThermoFisher, 1 μM/ml) in dark for 10 min and then fixed with 1 ml 4% paraformaldehyde

(PFA) in 1×PBS at 37°C for 5min. After washing with 1×PBS, at least 5 frames from each single infected well were randomly selected and imaged with Nikon Ti-E microscope, capturing 500 cells. All images were analysed with FIJI and experiments were repeated 3 times for biological replicates.

Filtered Titans phagocytosis assays: After 24h of in *vitro* induction, H99 titanised total population was passed through an 11μm filter to separate titan (>11μm) and typical cells (<11μm). Then both populations were washed, normalized and opsonize independently before adding to infection assays. Activation and infection of macrophages with opsonized *C. neoformans* cells followed the same protocol as described above.

Intracellular proliferation and vomocytosis assays. At time point 0 of phagocytosis assays, extracellular cells were removed by washing with warm fresh DMEM+. All samples were maintained at 37°C, 5%CO_2 in the Nikon Ti-E microscope chamber and imaged for 18h via time-lapse. Images were taken every 15 min and compiled into single movie files for analysis using NIS elements or FIJI software. Movies then were scored visually for intracellular proliferation rate, macrophage death and vomocytosis percentage. Vomocytosis scoring followed the guidelines described in Andrew et al., 2017 (40).

Secreted cytokine quantification: DuoSet ELISA Development kits from R&D Systems were used for all cytokine measurements according to the manufacturer's instructions. All media supernatants were directly used for ELISA, and the cytokine concentrations were determined by reference to a standard curve provided by the manufacturer.

Cell wall staining: Cells from 24 hr induced titan cultures were collected, washed twice with 1xPBS and resuspended in 500ul McIIvaine buffer. Cells were stained with EosinY (5μg/ml) in dark for 10mins and repeated for washes with McIIvaine buffer, then resuspended in 500ul 1×PBS. CFW (10 ug/ml) and ConA (50 ug/ml) were added into samples and maintained in the dark for 10 mins. After washing twice with 1×PBS, cells were imaged with a Zeiss Axio Observer and analysed for fluorescent intensities with Attune NxT Flow cytometer.

Flow cytometry for cell ploidy: Cells were fixed and stained according to the protocol of (15). Cells were fixed with 50% methanol for 15 mins, washed 3 times with 1×PBS and

stained with 3 ug/ml DAPI. Cells were analysed for DNA content using an Attune NxT Flow cytometer with violet laser. All flow cytometry data were analysed with FlowJo. Doublets and clumps were excluded using recommended gating system of FSC-H vs FSC-A, which was determined to be more parsimonious than SSC-H vs SSC-W followed by FSC-H vs. FSC-W. Autofluorescence in the DAPI channel was excluded by comparison to unstained cells. Gates for 1C and 2C were established with haploid controls cultured in YPD liquid media as described in the text.

Cell sizes measurement: Cell diameter was measured using FIJI, with frames randomly selected, all cells in a given frame analyzed, and at least 5 images acquired per sample for each of two independent runs. Total cell number of each samples was >200. All statistical analyses were performed using Graphpad Prism.

References

1. Park BJ, Wannemuehler KA, Marston BJ, Govender N, Pappas PG, Chiller TM. 2009. Estimation of the current global burden of cryptococcal meningitis among persons living with HIV/AIDS. AIDS (London, England) 23:525-530.
2. May RC, Stone NR, Wiesner DL, Bicanic T, Nielsen K. 2016. Cryptococcus: from environmental saprophyte to global pathogen. Nat Rev Microbiol 14:106-17.
3. Denham ST, Brown JCS. 2018. Mechanisms of Pulmonary Escape and Dissemination by Cryptococcus neoformans. J Fungi (Basel) 4.
4. Okagaki LH, Strain AK, Nielsen JN, Charlier C, Baltes NJ, Chrétien F, Heitman J, Dromer F, Nielsen K. 2010. Cryptococcal cell morphology affects host cell interactions and pathogenicity. PLoS Pathogens 6:e1000953.
5. Zaragoza O, Garcia-Rivera J, Nosanchuk JD, Cuenca-Estrella M, Rodriguez-Tudela J, Casadevall A. 2010. Fungal Cell Gigantism during Mammalian Infection. PLoS Pathogens 6:1-18.
6. Feldmesser M, Kress Y, Casadevall A. 2001. Dynamic changes in the morphology of Cryptococcus neoformans during murine pulmonary infection. Microbiology 147:2355-2365.
7. Love GL, Boyd GD, Greer DL. 1985. Large Cryptococcus neoformans isolated from brain abscess. J Clin Microbiol 22:1068-70.
8. Cruickshank JG, Cavill R, Jelbert M. 1973. Cryptococcus neoformans of unusual morphology. Appl Microbiol 25:309-12.
9. Zhou X, Ballou ER. 2018. The Cryptococcus neoformans Titan Cell: From In Vivo Phenomenon to In Vitro Model. Current Clinical Microbiology Reports 5:252-260.
10. Zaragoza O, Nielsen K. 2013. Titan cells in Cryptococcus neoformans: cells with a giant impact. Curr Opin Microbiol 16:409-13.
11. Gerstein AC, Fu MS, Mukaremera L, Li Z, Ormerod KL, Fraser JA, Berman J, Nielsen K. 2015. Polyploid titan cells produce haploid and aneuploid progeny to promote stress adaptation. MBio 6:e01340-15.

12. Mukaremera L, Lee KK, Wagener J, Wiesner DL, Gow NAR, Nielsen K. 2018. Titan cell production in Cryptococcus neoformans reshapes the cell wall and capsule composition during infection. The Cell Surface 1:15-24.
13. Wiesner DL, Specht CA, Lee CK, Smith KD, Mukaremera L, Lee ST, Lee CG, Elias JA, Nielsen JN, Boulware DR, Bohjanen PR, Jenkins MK, Levitz SM, Nielsen K. 2015. Chitin recognition via chitotriosidase promotes pathologic type-2 helper T cell responses to cryptococcal infection. PLoS Pathog 11:e1004701.
14. Crabtree JN, Okagaki LH, Wiesner DL, Strain AK, Nielsen JN, Nielsen K. 2012. Titan cell production enhances the virulence of Cryptococcus neoformans. Infect Immun 80:3776-85.
15. Dambuza IM, Drake T, Chapuis A, Zhou X, Correia J, Taylor-Smith L, LeGrave N, Rasmussen T, Fisher MC, Bicanic T, Harrison TS, Jaspars M, May RC, Brown GD, Yuecel R, MacCallum DM, Ballou ER. 2018. The Cryptococcus neoformans Titan cell is an inducible and regulated morphotype underlying pathogenesis. PLoS Pathog 14:e1006978.
16. Trevijano-Contador N, de Oliveira HC, García-Rodas R, Rossi SA, Llorente I, Zaballos Á, Janbon G, Ariño J, Zaragoza Ó. 2018. Cryptococcus neoformans can form titan-like cells in vitro in response to multiple signals that require the activation of several transduction pathways. PLoS Pathog 14:e1007007.
17. Hommel B, Mukaremera L, Cordero RJB, Desjardins CA, Sturny-Leclere A, Perfect JR ea. 2018. Identification of environmental and genetic factors important for Cryptococcus neoformans titan cell formation using new in vitro inducing conditions. PLoS Pathog.
18. Li Z, Nielsen K. 2017. Morphology Changes in Human Fungal Pathogens upon Interaction with the Host. J Fungi (Basel) 3.
19. Okagaki LH, Wang Y, Ballou ER, O'Meara TR, Bahn Y-S, Alspaugh JA, Xue C, Nielsen K. 2011. Cryptococcal titan cell formation is regulated by G-protein signaling in response to multiple stimuli. Eukaryotic Cell 10:1306-1316.
20. Evans RJ, Li Z, Hughes WS, Djordjevic JT, Nielsen K, May RC. 2015. Cryptococcal phospholipase B1 is required for intracellular proliferation and control of titan cell morphology during macrophage infection. Infect Immun 83:1296-304.
21. Mukaremera L, McDonald TR, Nielsen JN, Molenaar CJ, Akampurira A, Schutz C, Taseera K, Muzoora C, Meintjes G, Meya DB, Boulware DR, Nielsen K. 2019. The Mouse Inhalation Model of Cryptococcus neoformans Infection Recapitulates Strain Virulence in Humans and Shows that Closely Related Strains Can Possess Differential Virulence. Infection and Immunity 87.
22. Fernandes KE, Brockway A, Haverkamp M, Cuomo CA, van Ogtrop F, Perfect JR, Carter DA. 2018. Phenotypic Variability Correlates with Clinical Outcome in Cryptococcus Isolates Obtained from Botswanan HIV/AIDS Patients. MBio 9.
23. Vanhove M, Beale MA, Rhodes J, Chanda D, Lakhi S, Kwenda G, Molloy S, Karunaharan N, Stone N, Harrison TS, Bicanic T, Fisher MC. 2017. Genomic epidemiology of Cryptococcus yeasts identifies adaptation to environmental niches underpinning infection across an African HIV/AIDS cohort. Mol Ecol 26:1991-2005.
24. Molloy SF, Kanyama C, Heyderman RS, Loyse A, Kouanfack C, Chanda D, Mfinanga S, Temfack E, Lakhi S, Lesikari S, Chan AK, Stone N, Kalata N, Karunaharan N, Gaskell K, Peirse M, Ellis J, Chawinga C, Lontsi S, Ndong JG, Bright P, Lupiya D, Chen T, Bradley J, Adams J, van der Horst C, van Oosterhout JJ, Sini V, Mapoure YN, Mwaba P, Bicanic T, Lalloo DG, Wang D, Hosseinipour MC, Lortholary O, Jaffar S, Harrison TS, Team ATS. 2018. Antifungal Combinations for Treatment of Cryptococcal Meningitis in Africa. N Engl J Med 378:1004-1017.

25. Mylonakis E, Moreno R, El Khoury JB, Idnurm A, Heitman J, Calderwood SB, Ausubel FM, Diener A. 2005. Galleria mellonella as a model system to study Cryptococcus neoformans pathogenesis. Infect Immun 73:3842-50.
26. Garcia-Rodas R, Casadevall A, Rodriguez-Tudela JL, Cuenca-Estrella M, Zaragoza O. 2011. Cryptococcus neoformans capsular enlargement and cellular gigantism during Galleria mellonella infection. PLoS One 6:e24485.
27. Fernandes KE, Brockway A, Haverkamp M, Cuomo CA, van Ogtrop F, Perfect JR, Carter DA. 2018. Phenotypic Variability Correlates with Clinical Outcome in Cryptococcus Isolates Obtained from Botswanan HIV/AIDS Patients. mBio 9.
28. Galitski T, Saldanha AJ, Styles CA, Lander ES, Fink GR. 1999. Ploidy Regulation of Gene Expression. Science 285:251-254.
29. Mortimer RK. 1958. Radiobiological and Genetic Studies on a Polyploid Series (Haploid to Hexaploid) of Saccharomyces cerevisiae. Radiation Research 9:312-326.
30. Hickman MA, Paulson C, Dudley A, Berman J. 2015. Parasexual Ploidy Reduction Drives Population Heterogeneity Through Random and Transient Aneuploidy in Candida albicans. Genetics 200:781-94.
31. García-Rodas R, Cordero RJB, Trevijano-Contador N, Janbon G, Moyrand F, Casadevall A, Zaragoza O. 2014. Capsule growth in Cryptococcus neoformans is coordinated with cell cycle progression. mBio 5:e00945-14.
32. Ohkusu M, Raclavsky V, Takeo K. 2004. Induced synchrony in Cryptococcus neoformans after release from G2-arrest. Antonie van Leeuwenhoek 85:37-44.
33. Delobel P, Tesniere C. 2014. A simple FCM method to avoid misinterpretation in Saccharomyces cerevisiae cell cycle assessment between G0 and sub-G1. PLoS One 9:e84645.
34. Zhang J, Martinez-Gomez K, Heinzle E, Wahl SA. 2019. Metabolic switches from quiescence to growth in synchronized Saccharomyces cerevisiae. Metabolomics 15:121.
35. Ashton PM, Thanh LT, Trieu PH, Van Anh D, Trinh NM, Beardsley J, Kibengo F, Chierakul W, Dance DAB, Rattanavong S, Davong V, Hung LQ, Chau NVV, Tung NLN, Chan AK, Thwaites GE, Lalloo DG, Anscombe C, Nhat LTH, Perfect J, Dougan G, Baker S, Harris S, Day JN. 2019. Three phylogenetic groups have driven the recent population expansion of Cryptococcus neoformans. Nat Commun 10:2035.
36. Litvintseva AP, Kestenbaum L, Vilgalys R, Mitchell TG. 2005. Comparative analysis of environmental and clinical populations of Cryptococcus neoformans. J Clin Microbiol 43:556-64.
37. Zafar H, Altamirano S, Ballou ER, Nielsen K. 2019. A titanic drug resistance threat in Cryptococcus neoformans. Curr Opin Microbiol 52:158-164.
38. Johnston SA, May RC. 2013. Cryptococcus interactions with macrophages: evasion and manipulation of the phagosome by a fungal pathogen. Cellular Microbiology 15:403-411.
39. Rudman J, Evans RJ, Johnston SA. 2019. Are macrophages the heroes or villains during cryptococcosis? Fungal Genet Biol 132:103261.
40. Gilbert AS, Seoane PI, Sephton-Clark P, Bojarczuk A, Hotham R, Giurisato E, Sarhan AR, Hillen A, Velde GV, Gray NS, Alessi DR, Cunningham DL, Tournier C, Johnston SA, May RC. 2017. Vomocytosis of live pathogens from macrophages is regulated by the atypical MAP kinase ERK5. Sci Adv 3:e1700898.
41. Ma H, May RC. 2009. Virulence in Cryptococcus species. Adv Appl Microbiol 67:131-90.

42. Davis MJ, Eastman AJ, Qiu Y, Gregorka B, Kozel TR, Osterholzer JJ, Curtis JL, Swanson JA, Olszewski MA. 2015. Cryptococcus neoformans–Induced Macrophage Lysosome Damage Crucially Contributes to Fungal Virulence. The Journal of Immunology 194:2219-2231.
43. Alvarez M, Casadevall A. 2006. Phagosome extrusion and host-cell survival after Cryptococcus neoformans phagocytosis by macrophages. Curr Biol 16:2161-5.
44. Ma H, Croudace JE, Lammas DA, May RC. 2006. Expulsion of live pathogenic yeast by macrophages. Curr Biol 16:2156-60.
45. Davis MJ, Tsang TM, Qiu Y, Dayrit JK, Freij JB, Huffnagle GB, Olszewski MA. 2013. Macrophage M1/M2 polarization dynamically adapts to changes in cytokine microenvironments in Cryptococcus neoformans infection. mBio 4:e00264-13.
46. Leopold Wager CM, Wormley FL, Jr. 2014. Classical versus alternative macrophage activation: the Ying and the Yang in host defense against pulmonary fungal infections. Mucosal Immunol 7:1023-35.
47. Serbina NV, Jia T, Hohl TM, Pamer EG. 2008. Monocyte-mediated defense against microbial pathogens. Annu Rev Immunol 26:421-52.
48. Lauvau G, Loke P, Hohl TM. 2015. Monocyte-mediated defense against bacteria, fungi, and parasites. Semin Immunol 27:397-409.
49. Heung LJ, Hohl TM. 2019. Inflammatory monocytes are detrimental to the host immune response during acute infection with Cryptococcus neoformans. PLoS Pathog 15:e1007627.
50. Lauvau G, Soudja SM. 2015. Mechanisms of Memory T Cell Activation and Effective Immunity. Adv Exp Med Biol 850:73-80.
51. Gordon S, Taylor PR. 2005. Monocyte and macrophage heterogeneity. Nat Rev Immunol 5:953-64.
52. Taylor PR, Gordon S. 2003. Monocyte heterogeneity and innate immunity. Immunity 19:2-4.
53. Erwig LP, Gow NA. 2016. Interactions of fungal pathogens with phagocytes. Nat Rev Microbiol 14:163-76.
54. Probert M, Zhou X, Goodall M, Johnston SA, Bielska E, Ballou ER, May RC. 2019. A Glucuronoxylomannan Epitope Exhibits Serotype-Specific Accessibility and Redistributes towards the Capsule Surface during Titanization of the Fungal Pathogen Cryptococcus neoformans. Infection and Immunity 87.
55. Sionov E, Lee H, Chang YC, Kwon-Chung KJ. 2010. Cryptococcus neoformans overcomes stress of azole drugs by formation of disomy in specific multiple chromosomes. PLoS Pathog 6:e1000848.
56. Ngamskulrungroj P, Chang Y, Hansen B, Bugge C, Fischer E, Kwon-Chung KJ. 2012. Characterization of the chromosome 4 genes that affect fluconazole-induced disomy formation in Cryptococcus neoformans. PLoS One 7:e33022.
57. Sionov E, Chang YC, Kwon-Chung KJ. 2013. Azole heteroresistance in Cryptococcus neoformans: emergence of resistant clones with chromosomal disomy in the mouse brain during fluconazole treatment. Antimicrob Agents Chemother 57:5127-30.
58. Stone NR, Rhodes J, Fisher MC, Mfinanga S, Kivuyo S, Rugemalila J, Segal ES, Needleman L, Molloy SF, Kwon-Chung J, Harrison TS, Hope W, Berman J, Bicanic T. 2019. Dynamic ploidy changes drive fluconazole resistance in human cryptococcal meningitis. J Clin Invest 129:999-1014.

59. Semighini CP, Averette AF, Perfect JR, Heitman J. 2011. Deletion of Cryptococcus neoformans AIF ortholog promotes chromosome aneuploidy and fluconazole-resistance in a metacaspase-independent manner. PLoS Pathogens 7:e1002364.
60. Hickman MA, Zeng G, Forche A, Hirakawa MP, Abbey D, Harrison BD, Wang YM, Su CH, Bennett RJ, Wang Y, Berman J. 2013. The 'obligate diploid' Candida albicans forms mating-competent haploids. Nature 494:55-9.
61. Todd RT, Wikoff TD, Forche A, Selmecki A. 2019. Genome plasticity in Candida albicans is driven by long repeat sequences. Elife 8.
62. Forche A, Abbey D, Pisithkul T, Weinzierl MA, Ringstrom T, Bruck D, Petersen K, Berman J. 2011. Stress alters rates and types of loss of heterozygosity in Candida albicans. mBio 2.
63. Forche A, Cromie G, Gerstein AC, Solis NV, Pisithkul T, Srifa W, Jeffery E, Abbey D, Filler SG, Dudley AM, Berman J. 2018. Rapid Phenotypic and Genotypic Diversification After Exposure to the Oral Host Niche in Candida albicans. Genetics 209:725-741.
64. Okagaki LH, Nielsen K. 2012. Titan cells confer protection from phagocytosis in Cryptococcus neoformans infections. Eukaryot Cell 11:820-6.
65. Campuzano A, Wormley FL. 2018. Innate Immunity against Cryptococcus, from Recognition to Elimination. J Fungi (Basel) 4.
66. Probert M, Zhou X, Goodall M, Johnston SA, Bielska E, Ballou ER, May RC. 2019. A Glucuronoxylomannan Epitope Exhibits Serotype-Specific Accessibility and Redistributes towards the Capsule Surface during Titanization of the Fungal Pathogen Cryptococcus neoformans. Infect Immun 87.

Figure 1: Titan cells formation varies among clinical isolates. (**A**) *C. neoformans* cells from the indicated strains were grown under inducing conditions for 24 hours and then visualized by light microscopy. Cell size was assessed for individual cells (diameter) for the cell body (capsule excluded). The presence of cells >10 μm was taken as in indication of titanization capacity. (**B**) *C. neoformans* cells from the indicated strains were grown under inducing conditions for 24h and stained with calcofluor white (CFW) to reveal cell wall. Cell size was assessed for individual cells (diameter) for the cell body (capsule excluded) (n>200). (**C**) *C. neoformans* cells from the indicated strains were grown under inducing conditions for 24h and then fixed and analysed for size by flow cytometry, with FSC-A as a proxy for cell size. Single cells were identified by FSC-A vs FSC-H to remove doublets (n>8000 after gating). i) H99 and Zc8 populations are shown with the distinct shoulder indicative of population structure consistent with titan cells highlighted in grey. ii) Histograms for cell size (FSC-A) are shown for all four isolates. The dotted line indicates the size threshold identified for H99 cells with DNA content >4C. iii) FSC-A vs SSC-A scatter plots for H99 and Zc8 populations. (**D**) *C. neoformans* cells from the indicated strains were grown under inducing conditions for 24h, then fixed and stained with DAPI and analysed by flow cytometry for DNA content. Single cells were identified by FSC-A vs FSC-H to remove doublets (n>8000 after gating). 1C and 2C populations were identified relative to YPD grown yeast cells from matched parent strains and Median Fluorescence Intensity was recorded for 1C and 2C peaks. (**E**) Mating fronts from the indicated isolates crossed with KN99**a** were excised, fixed, stained with DAPI, and analyzed by flow cytometry for DNA content. Single cells were identified by FSC-A vs FSC-H to remove doublets (n>500 after gating). 1C and 2C populations were identified relative to YPD-agar grown yeast cells from matched parent strains and Median Fluorescence Intensity was recorded for sub-1C, 1C, 2C peaks.

Figure 2: Disease outcomes on mice model varied among clinical isolates. Mice were infected intranasally with the indicated strains and sacrificed on day 10 for analysis of CFUs and immune cell recruitment. (**A**) Size analysis of fungal cells collected from murine lungs. For each isolate, lung homogenates from 3 independent mice were inspected for the presence of titan cells. Fungal cells were fixed and stained with CFW and visualized by light microscopy (n>70 cells for each isolate). Data were assessed for normality by Shapiro-Wilk and H99 and Zc8 distributions were compared using the non-parametric Kolmogorov-Smirnov test. (**B,C**) Infectious burdens for the indicated strains. Murine lungs (B) and brains (C) were assessed for dissemination 10 days post-infection via colony forming unit of total homogenates (n=5 per strain). Data are presented as Log CFU/gram. (**B**) Data were assessed as normal by Shapiro-Wilk and analysed by One-Way ANOVA with Holm-Sidak's multiple comparisons test. Data are presented as Log CFU/gram. (**C**) Data were assessed as not normal by Shapiro-Wilk and analysed by Kruskal-Wallis ANOVA with Dunn's correction for multiple comparisons. (**D,E**) Immune cell recruitment to lungs for the indicated strains. Lung homogenates were analysed by FACS for the indicated cell populations identified using the indicated markers for (D) Neutrophils (CD45+, CD11b+Ly6G+) or (E) Alveolar Macrophages (CD45+ Ly6C- Ly6G- CD11b- SiglecF+). Data were assessed as normal by Shapiro-Wilk and analysed by One-Way ANOVA with Holm-Sidak's multiple comparisons test.

Figure 3 Clinical isolates produce aneuploid daughter cells with altered drug resistance *in vivo*. (A) Degree of heterogeneity in ploidy across the individual colony forming units recovered from host tissue Individual colonies recovered from the indicated organs were fixed and stained with DAPI and analysed by flow cytometry. Single cells were identified by FSC-A vs FSC-H to remove doublets (n>8000 after gating). 1C and 2C populations were identified relative to YPD-grown colonies from matched parent strains and Median Fluorescence Intensity was recorded for 1C and 2C peaks. Data are presented relative to median 1C MFI for all colonies for a given isolate. Data were assessed as not normal by Shapiro-Wilk and analysed by Kruskal-Wallis ANOVA compared to H99 with Dunn's correction for multiple comparisons. (B) Fluconazole resistance relative to parent for individual colonies aggregated in (A). Individual colonies were propagated overnight in YNB for 18 hours and then normalized to 0.1 OD in YNB and assessed for Fluconazole MIC after 48 hours. Data are plotted relative to parent MIC and as a function of colony ploidy as assessed in (A). Data were assessed as not normal by Shapiro-Wilk and analysed by Kruskal-Wallis ANOVA with Dunn's correction for multiple comparisons.

Figure 4: *In vitro* Titan cells interaction with host immune cells. (**A-D**) Infection rates for the 4 clinical strains, showing the percentage of macrophages infected with at least one internalized *C. neoformans* cell after 2h co-incubation. (**A**) 400 macrophages were assessed for each biological replicate (n=3), and data for a single representative biological replicate is presented. Data were assessed as not normal by Shapiro-Wilk and analysed by Welch's ANOVA with Dunnett's test for multiple comparisons. *p<0.02; ***p=0.0008 "T" indicates pre-titanized cells. (**B**) Representative images showing macrophages infected with cryptococcal cells. Scale bar: 10 μm. (**C**) Representative images showing macrophages infected with H99 yeast and titan cells. Macrophages were incubated with lysotracker (Red). Fungi were co-incubated with anti-capsule antibody 18b7 plus anti-mouse IgG-FITC (Green) and calcofluor white (CFW) for chitin (blue). Scale bar: 20μm. (**D**) Macrophages were co-incubated for 2 hours with pre-titanized *C. neoformans* that had been filtered by size (typical cells <10 um, Titan cells > 11 μm). 500 macrophages were assessed for each biological replicate, and data for a single representative biological replicate is presented (n>3). Data were assessed for normality by Shapiro-Wilk and analysed by Student's T-test with Welsh's correction for unequal variance (determined by F-test). ***p=0.0002. (**E-H**) Macrophages and pre-titanized *C. neoformans* were co-incubated for 18 hours and assessed via live imaging for (**E**) IPR, (**F**) vomocytosis, and (**G**) macrophage lysis. 400 macrophages were assessed for each biological replicate (n>3), and data for a single representative biological replicate is presented. (**E**) IPR: mean intracellular proliferation rate. Data were assessed for normality by Shapiro-Wilk and analysed by One-Way ANOVA. (**F**) Mϕ death %: frequency of macrophage death indicated by cell lysis. Data were assessed for normality by Shapiro-Wilk and analysed by One-Way ANOVA. *p=0.05; ***p<0.001. (**G**) Vomo %: frequency of vomocytosis. Data were assessed as not normal by Shapiro-Wilk and analysed by Kruskal-Wallis with Dunn's correction. **(H**) H_2O_2 resistance. Cells from the indicated strains were grown under inducing conditions for 18hr or in YNB overnight (0h), then plated in 10-fold serial dilutions from OD=0.1 onto YNB or YNB plus 0.5mM H_2O_2. Plates were incubated at 30°C for 2 days and then imaged.

Figure 5. Titan cells enhance the production of TNF. (**A**) J774.1 Macrophages and YNB-grown or pre-titanized *C. neoformans* of the indicated strains were co-incubated for 24 hours in triplicate. Supernatants were collected and TNF measured. Data for a representative biological replicate is presented (n>3). Data were assessed for normality by Shapiro-Wilk and analysed by One-Way ANOVA with Holm-Sidak's correction for multiple comparison. **p=0.004; ***p<0.001; ****p<0.0001. (**B**) J774.1 Macrophages were co-incubated with pre-titanized H99 *C. neoformans* that had been filtered by size (typical cells <10 um > titan) for 24 hours in triplicate. Supernatants were collected and TNF measured. Data for a representative biological replicate is presented (n>3). Data were assessed for normality by Shapiro-Wilk and analysed by One-Way ANOVA with Tukey's correction for multiple comparison. (**C**) Human monocytes from whole blood and YNB-grown or pre-titanized *C. neoformans* of the indicated strains were co-incubated for 4 or 24 hours plus or minus IFNγ 10U/ml in triplicate. LPS-treated monocytes (100ng/ml 24hr) served as a positive control. Supernatants were collected and TNFα measured. Data for a representative biological replicate is presented (n>3). Data were analysed by Two-Way ANOVA with Tukey's correction for multiple comparison.

Figure 6: Capsule size and composition are affected by titan induction. (A) Pre-titanised cells of indicated strains were exposed to IgM primary antibody (Crp127) then anti-IgM FITC(Green) secondary body; imaged with India ink staining for overall capsule structure; bar scale: 10μm. (B) Total capsule and cell body diameters were measured and a ratio reported for each cell. Data were assessed as not normal by Shapiro-Wilk and analysed by Kruskal-Wallis with Dunn's correction (n>100). ****: p<0.0001. (C,D) IgM staining was analysed by flow cytometry, gating on single cells as previously described (n>8000 single cell for all isolates), with frequency and MFI reported for . Di) Gates show peaks for different levels of staining, with corresponding Median Fluorescence Intensity indicated in (C). Dotted lines indicate proportion of cells that failed to bind Crp127 IgM (%Neg). Dii) Size (FSC-A) vs IgM-FITC intensity, with different populations highlighted as in (Ci). For all figures, data for a representative biological replicate is presented (n>3).

Figure 7. Non-titanising strains also exhibit population heterogeneity. (A) Cells from the indicated strains were grown under inducing conditions for 24h or in YNB overnight, then stained for different PAMPs: Mannan (ConA, Red), Chitosan (EosinY, Green), Chitin (CFW, Blue). YNB grown yeast scale bar 5µm; titanized cells scale bar 10 µm. (B) Stained cells from (A) were analysed by flow cytometery to determine Median Fluorescent Intensity indicating exposure of Chitin (CFW, right); Mannan (ConA, center); and Chitonsan (EosinY, left). (C) Cells from the indicated strains were grown under inducing conditions for 72h, then stained for different PAMPs and analysed by flow cytometery to determine Median Fluorescent Intensity indicating exposure of Chitin (CFW, right); Mannan (ConA, center); and Chitonsan (EosinY, left).

Supplemental Figures

Figure S1 (**A**) Indicated strains were mixed and incubated on Murashige Skoog agar in the dark at room temperature for up to 3 months. Images were acquired by light microscope equipped with a Levenhuk M35 Base Digital Camera at 20X magnification. (**B**) Indicated strains were pre-grown in the indicated conditions (YPD overnight or titan-inducing for 24 hours) and injected into the proleg of *Galleria mellonella* worms at 10^5 cells per worm (n=10). Worms were monitored daily for survival for up to 10 days. Survival was analysed by Kaplan-Meyer survival curve and significance was assessed by Log rank (Mantel-Cox) test (*=$p<0.05$). (**C**) Indicated strains were incubated overnight in YPD and then fixed and stained with DAPI and analysed by flow cytometry. Single cells were identified by FSC-A vs FSC-H to remove doublets (n>8000 after gating). 1C and 2C populations are indicated, along with the median fluorescence intensity (MFI) for each.

Figure S2 (**A**) Gating strategy for identification of cell populations presented in Figure 2. (**B**) Lung homogenates were analysed by FACS for the intersticial macrophages identified using markers for CD45+ Ly6G- Ly6C- cells.

Figure S3: Cells from the indicated strains in Figure 7 were grown under inducing conditions for 24h or in YNB overnight, then fixed and stained for different PAMPs. (**A**) i) *C. neoformans* cells were analysed for size by flow cytometry, with FSC-A as a proxy for cell size. Single cells were identified by FSC-A vs FSC-H to remove doublets (n>8000 after gating). ii) H99 and Zc8 populations are shown with the distinct shoulder indicative of population structure consistent with titan cells highlighted in grey. iii) FSC-A vs SSC-A scatter plots for H99 and Zc8 populations. (**B**) Stained cells from (A) were analysed by flow cytometery to determine Median Fluorescent Intensity indicating exposure of Chitin (CFW, right); Mannan (ConA, center); and Chitonsan (EosinY, left).

A

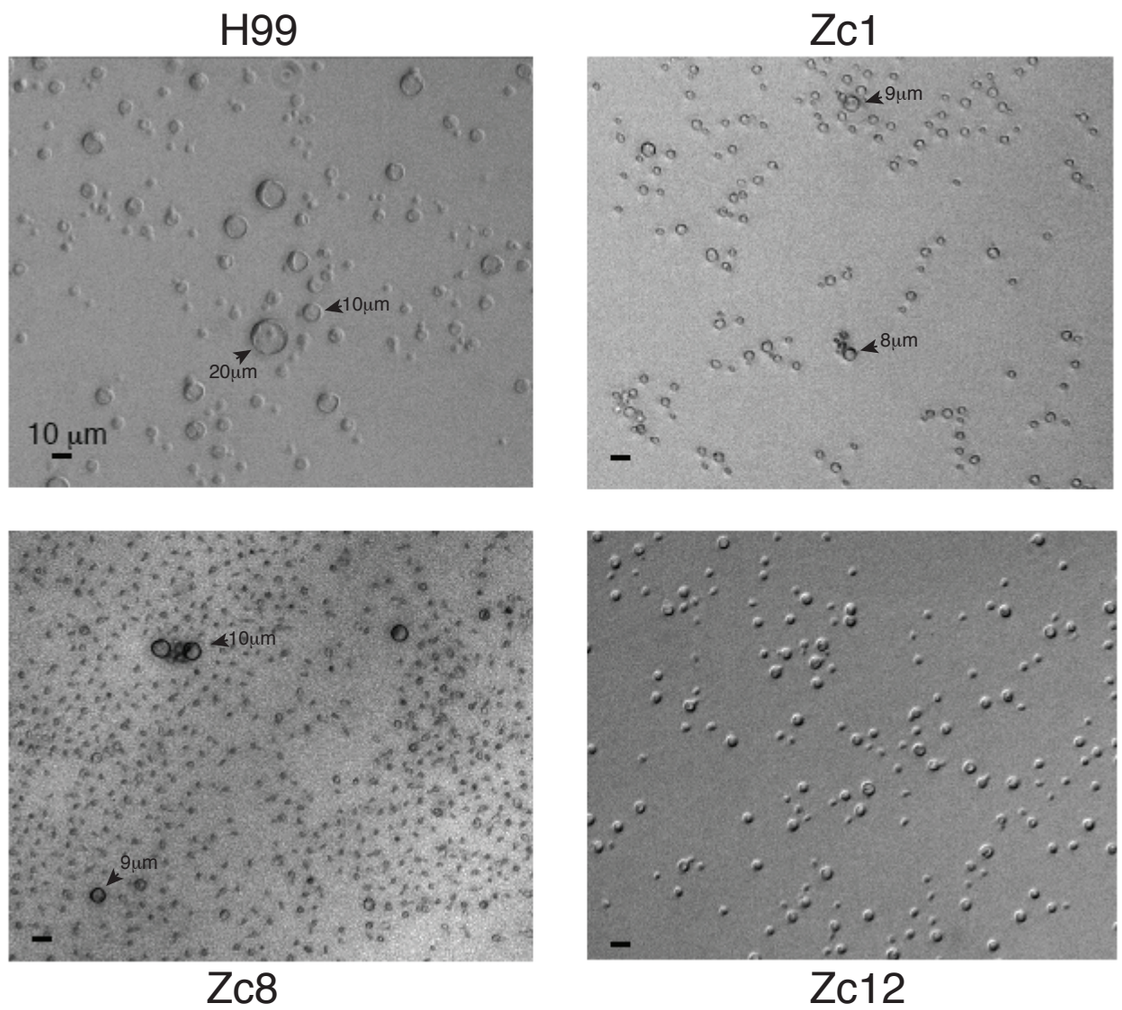
H99
Zc1
Zc8
Zc12
10 μm
20μm
10μm
9μm
8μm

B

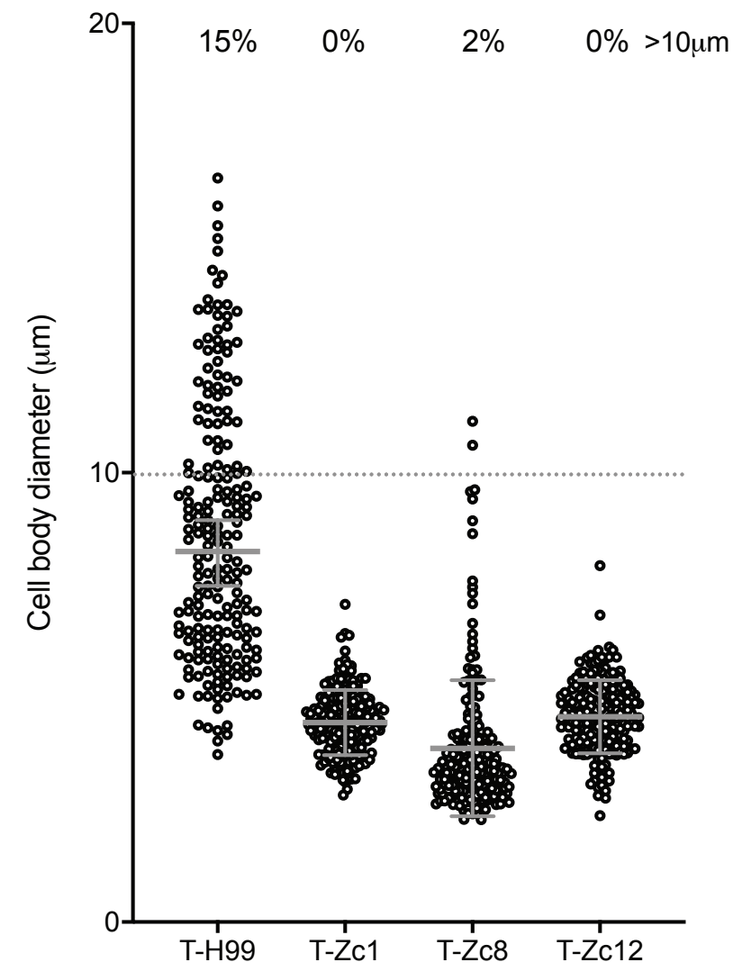
15%
0%
2%
0% >10μm
Cell body diameter (μm)
20
10
0
T-H99
T-Zc1
T-Zc8
T-Zc12

C

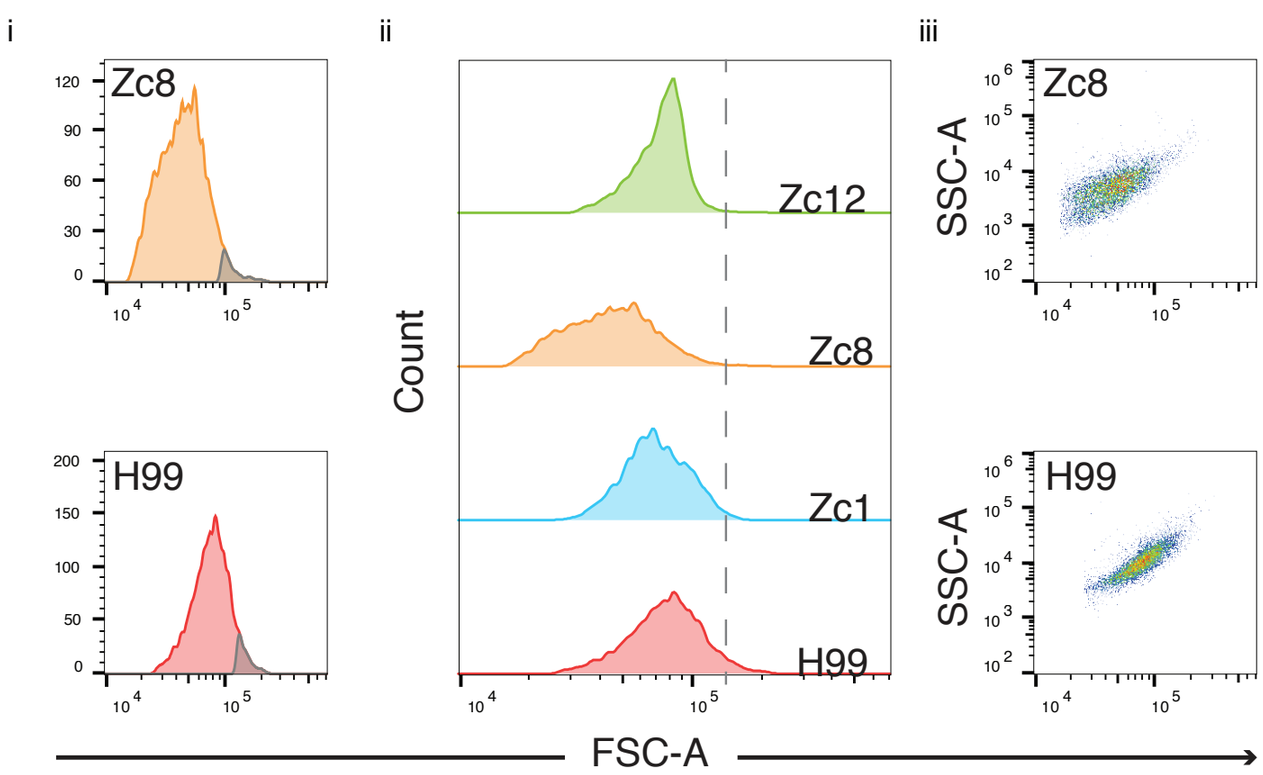
i
ii
iii
Zc8
H99
Count
Zc12
Zc8
Zc1
H99
SSC-A
FSC-A

D

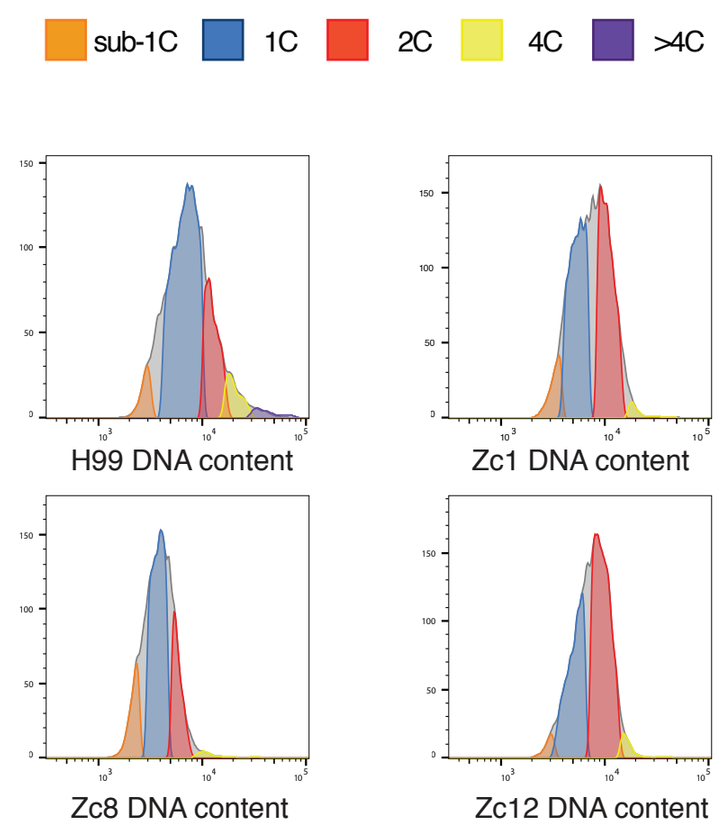
sub-1C
1C
2C
4C
>4C
H99 DNA content
Zc1 DNA content
Zc8 DNA content
Zc12 DNA content

E

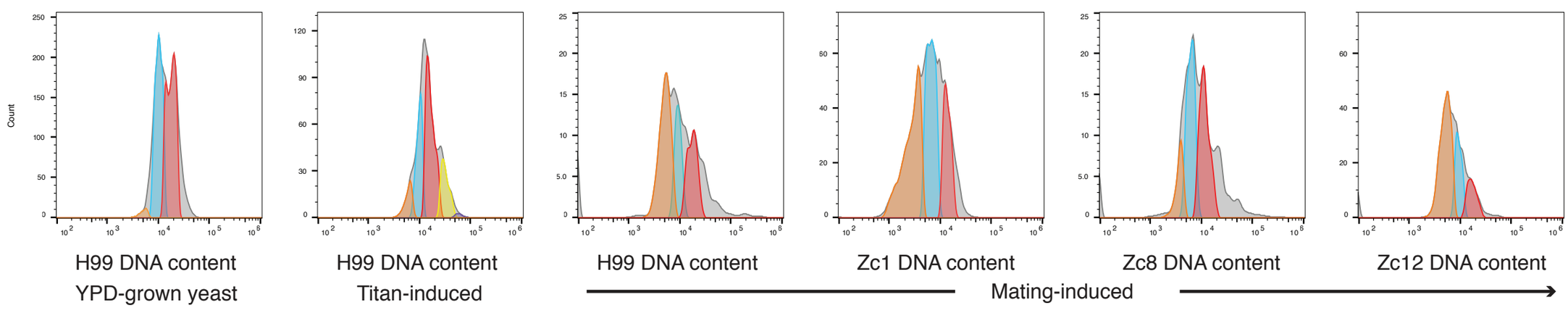
Count
H99 DNA content
YPD-grown yeast
H99 DNA content
Titan-induced
H99 DNA content
Zc1 DNA content
Zc8 DNA content
Zc12 DNA content
Mating-induced

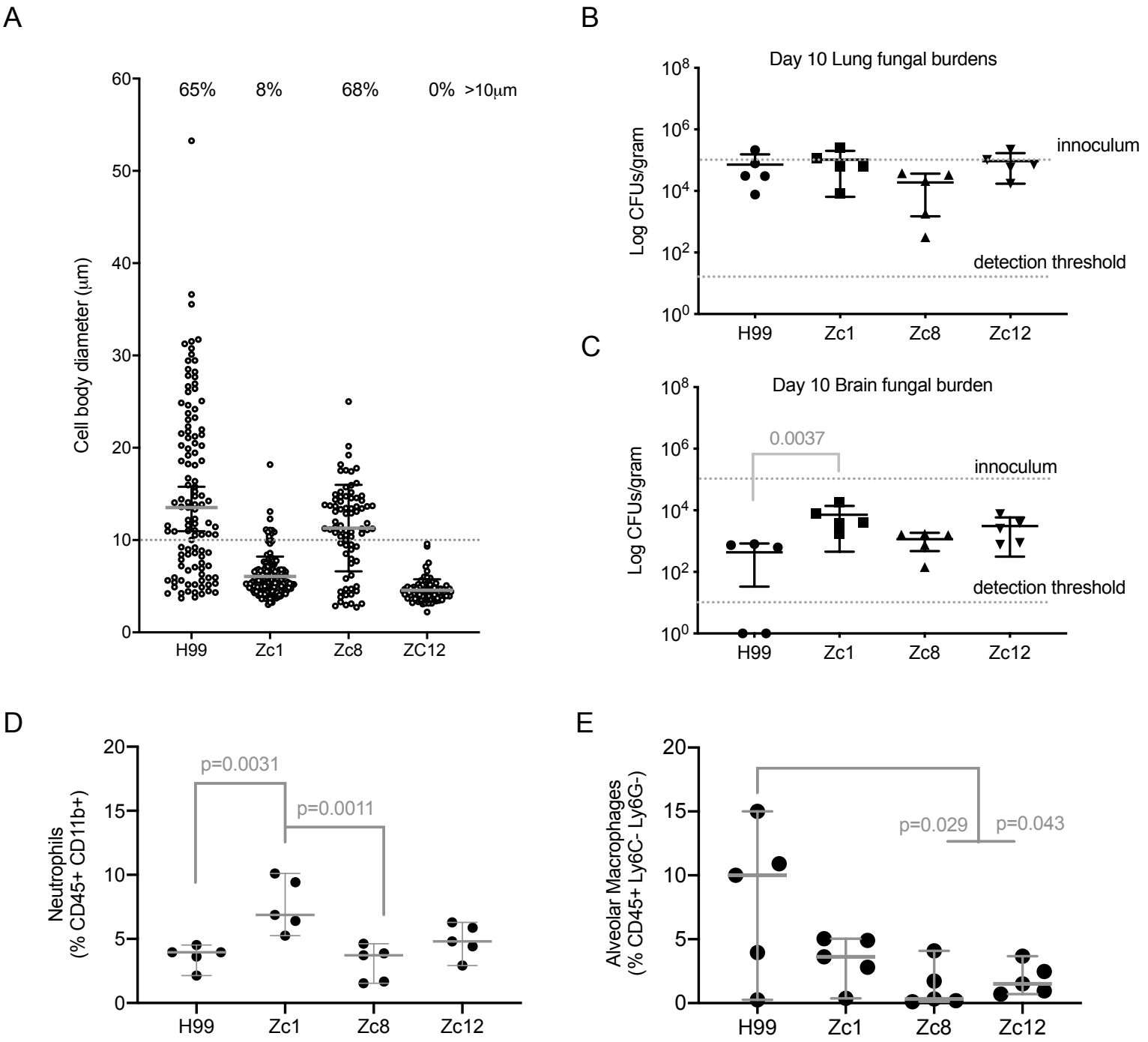
A
65%
8%
68%
0% >10μm
Cell body diameter (μm)
H99
Zc1
Zc8
ZC12
B
Day 10 Lung fungal burdens
Log CFUs/gram
innoculum
detection threshold
H99
Zc1
Zc8
Zc12
C
Day 10 Brain fungal burden
0.0037
Log CFUs/gram
innoculum
detection threshold
H99
Zc1
Zc8
Zc12
D
p=0.0031
p=0.0011
Neutrophils
(% CD45+ CD11b+)
H99
Zc1
Zc8
Zc12
E
p=0.029
p=0.043
Alveolar Macrophages
(% CD45+ Ly6C- Ly6G-)
H99
Zc1
Zc8
Zc12

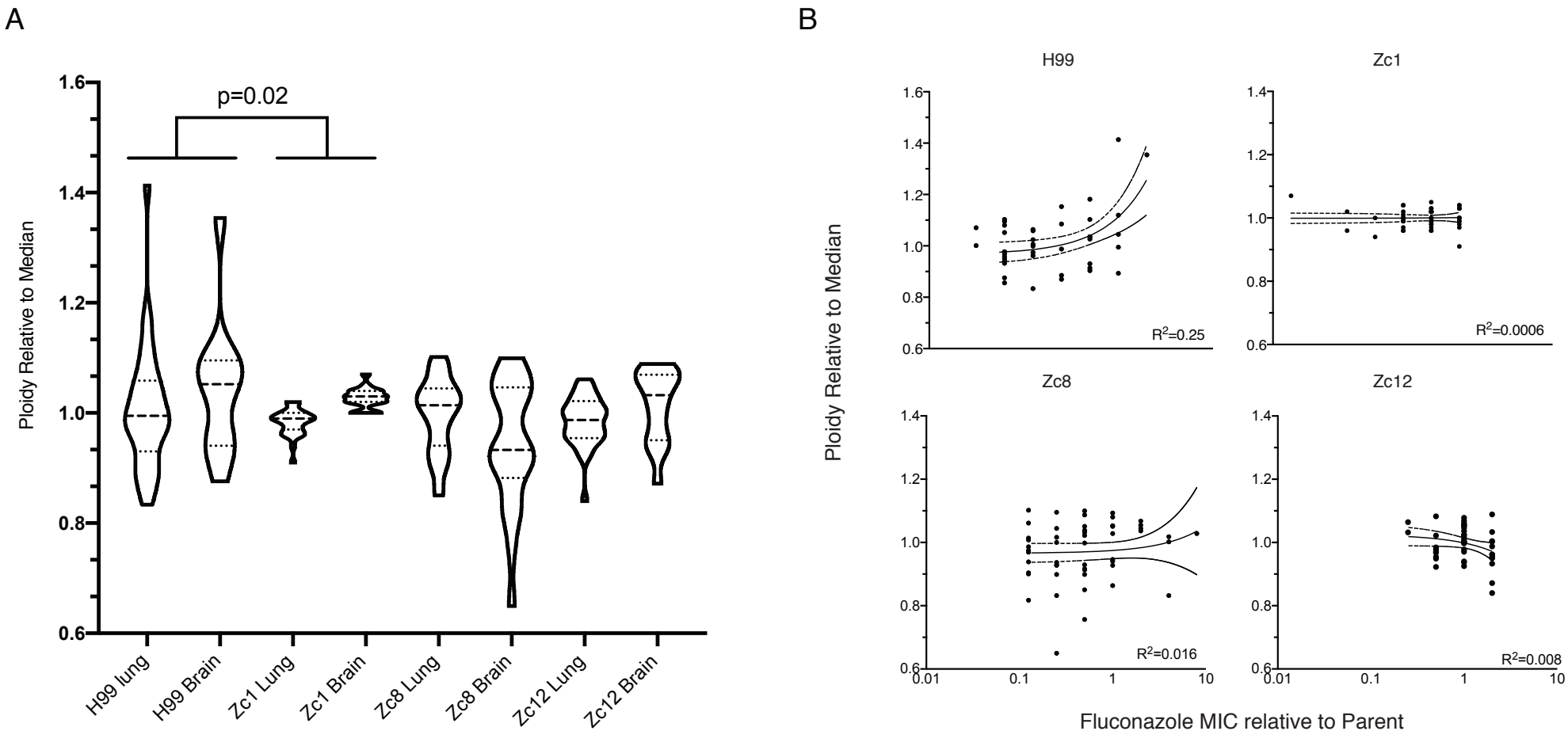
A
p=0.02
Ploidy Relative to Median
1.6
1.4
1.2
1.0
0.8
0.6
H99 lung
H99 Brain
Zc1 Lung
Zc1 Brain
Zc8 Lung
Zc8 Brain
Zc12 Lung
Zc12 Brain
B
H99
Zc1
Zc8
Zc12
R2=0.25
R2=0.0006
R2=0.016
R2=0.008
0.01
0.1
1
10
Fluconazole MIC relative to Parent

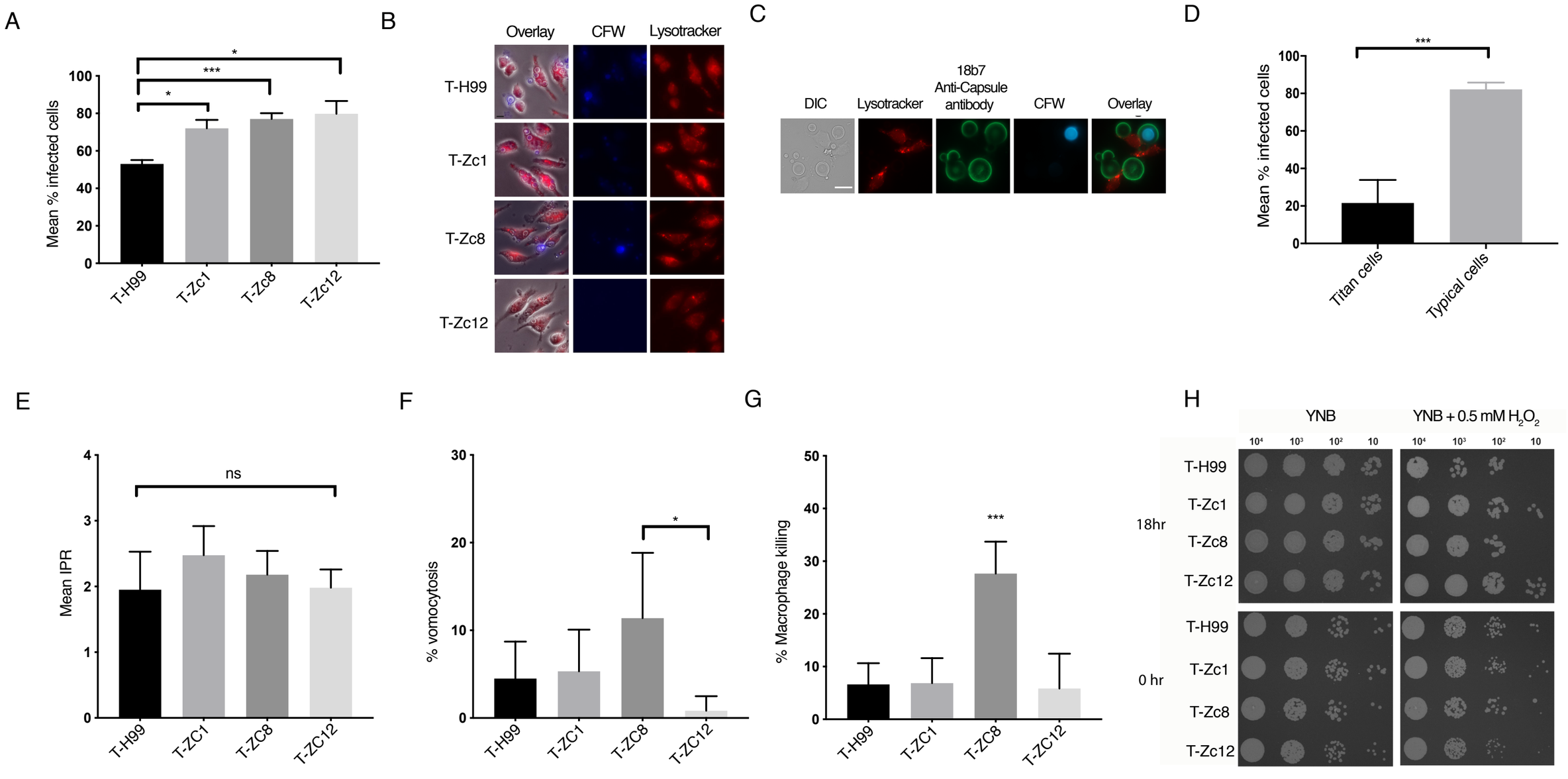
A
Mean % infected cells
100
80
60
40
20
0
*
***
*
T-H99
T-Zc1
T-Zc8
T-Zc12
B
Overlay
CFW
Lysotracker
T-H99
T-Zc1
T-Zc8
T-Zc12
C
DIC
Lysotracker
18b7
Anti-Capsule
antibody
CFW
Overlay
D
Mean % infected cells
100
80
60
40
20
0
***
Titan cells
Typical cells
E
Mean IPR
4
3
2
1
0
ns
T-H99
T-ZC1
T-ZC8
T-ZC12
F
% vomocytosis
30
20
10
0
*
T-H99
T-ZC1
T-ZC8
T-ZC12
G
% Macrophage killing
50
40
30
20
10
0
***
T-H99
T-ZC1
T-ZC8
T-ZC12
H
YNB
YNB + 0.5 mM H_2O_2
10^4
10^3
10^2
10
18hr
0 hr
T-H99
T-Zc1
T-Zc8
T-Zc12

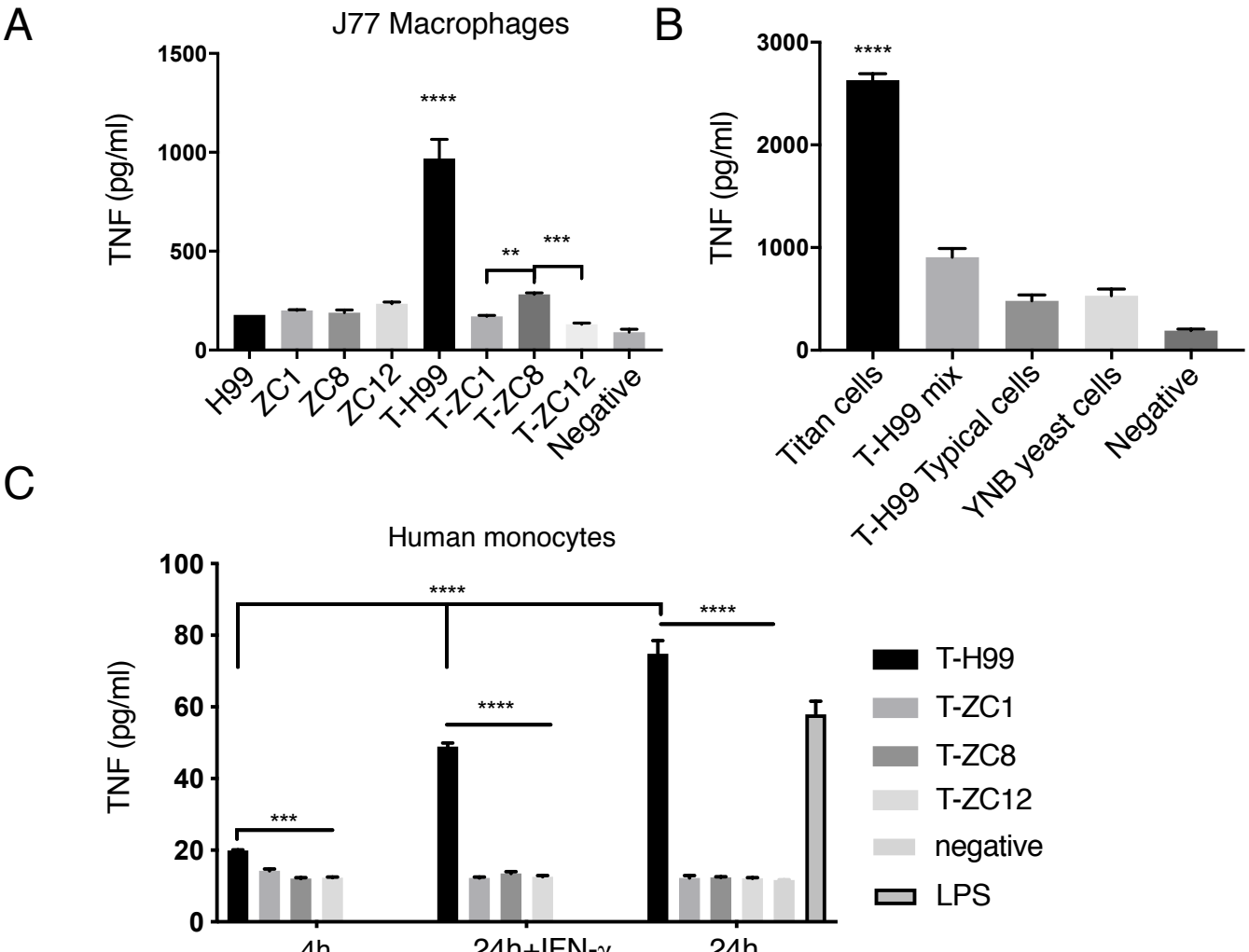
A
J77 Macrophages
TNF (pg/ml)
1500
1000
500
0
****
**
***
H99
ZC1
ZC8
ZC12
T-H99
T-ZC1
T-ZC8
T-ZC12
Negative
B
TNF (pg/ml)
3000
2000
1000
0
****
Titan cells
T-H99 mix
T-H99 Typical cells
YNB yeast cells
Negative
C
Human monocytes
TNF (pg/ml)
100
80
60
40
20
0
****
****
****
***
4h
24h+IFN-γ
24h
T-H99
T-ZC1
T-ZC8
T-ZC12
negative
LPS

A

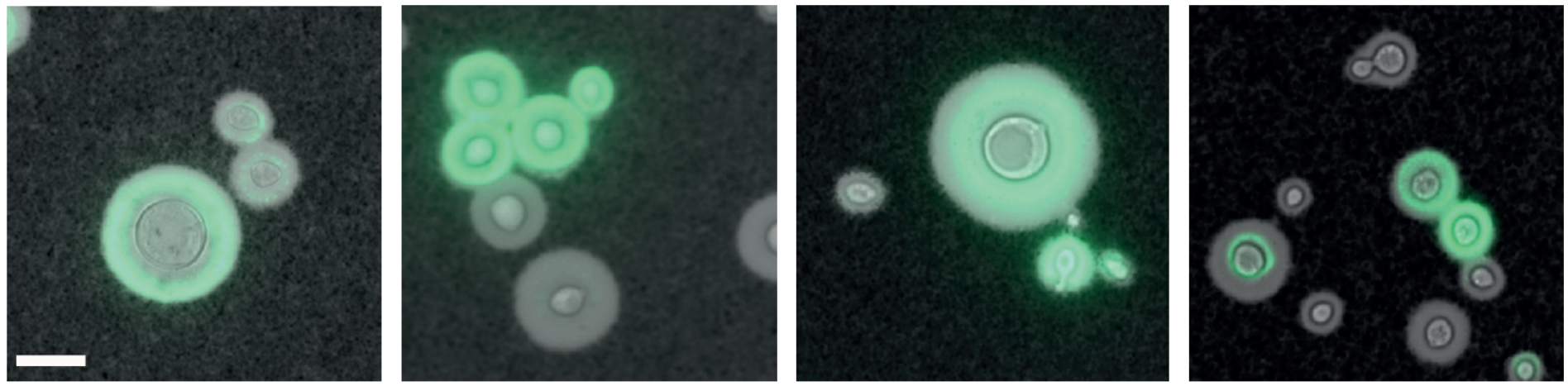

B

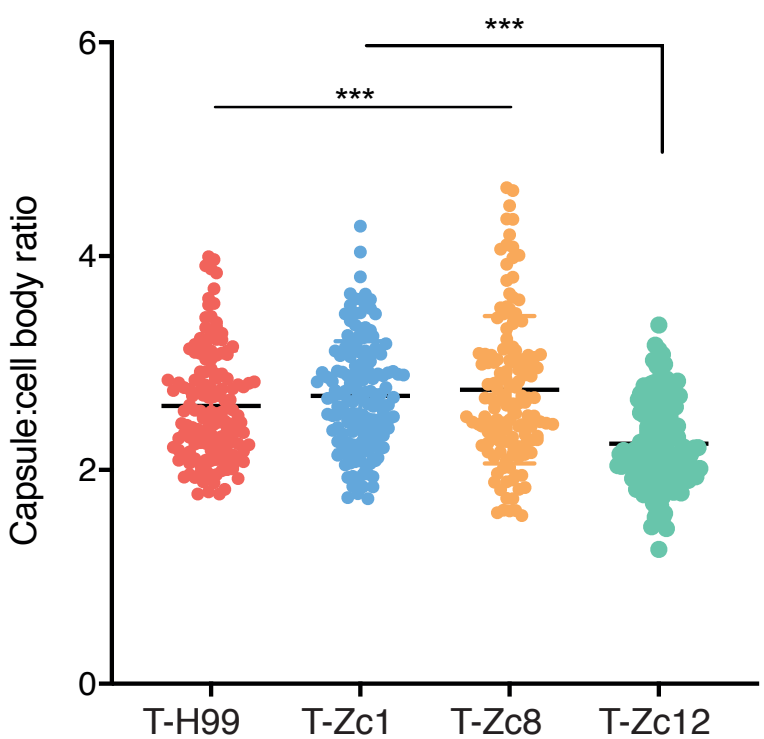

C

Crp127 IgM-FITC binding (MFI)

	T-H99	T-Zc1	T-Zc8	T-Zc12
(% Neg)	(36.9)	(63.1)	(94.3)	(39.9)
Low (%)	420 (18.9)	528 (9.52)	220 (4.55)	345 (47.5)
Med (%)	1955 (23.8)	1693 (24.6)	1385 (0.07)	1134 (8.78)
High (%)	5601 (18.9)	4533 (1.33)	N/A	5234 (0.72)

D

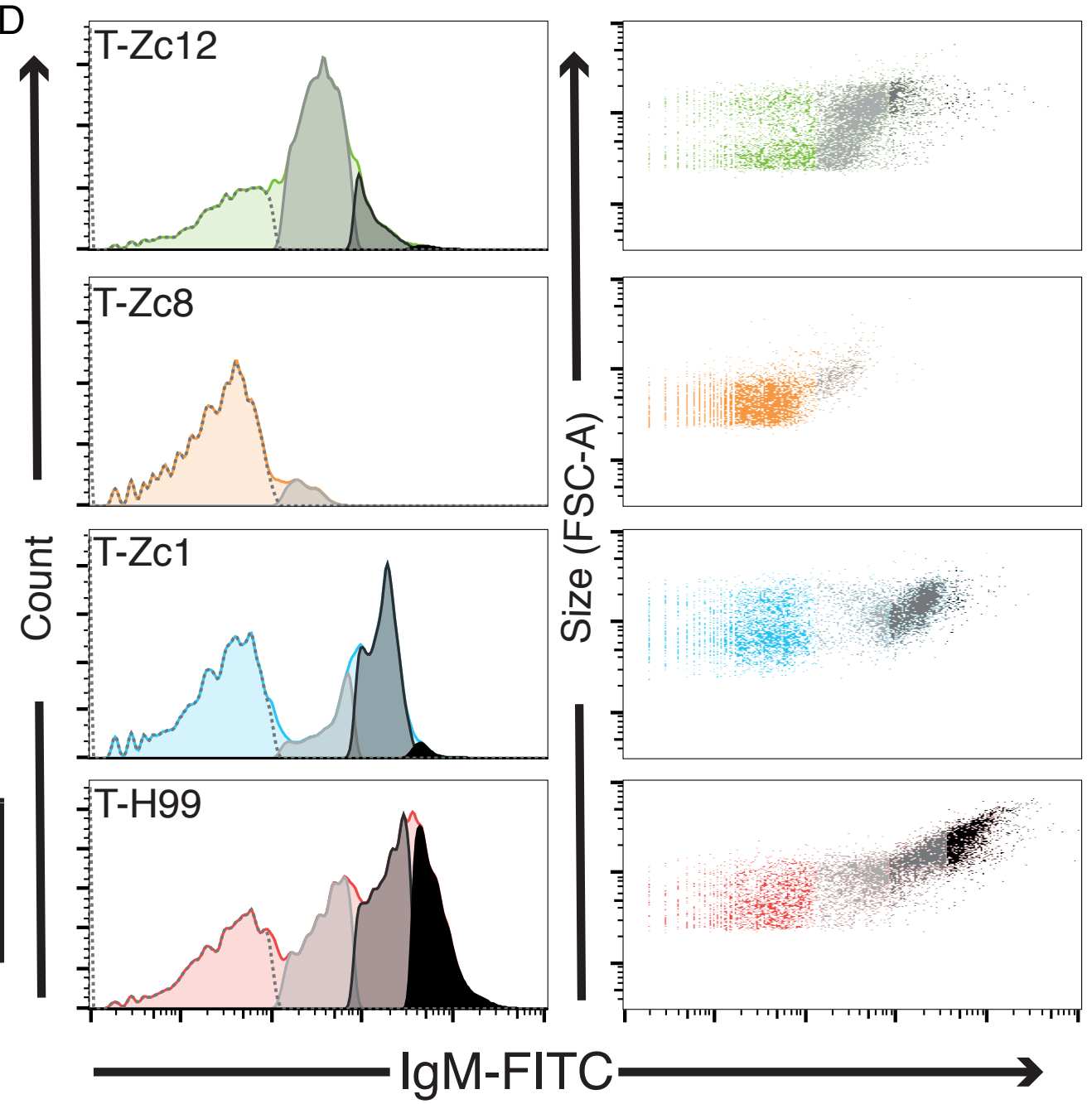

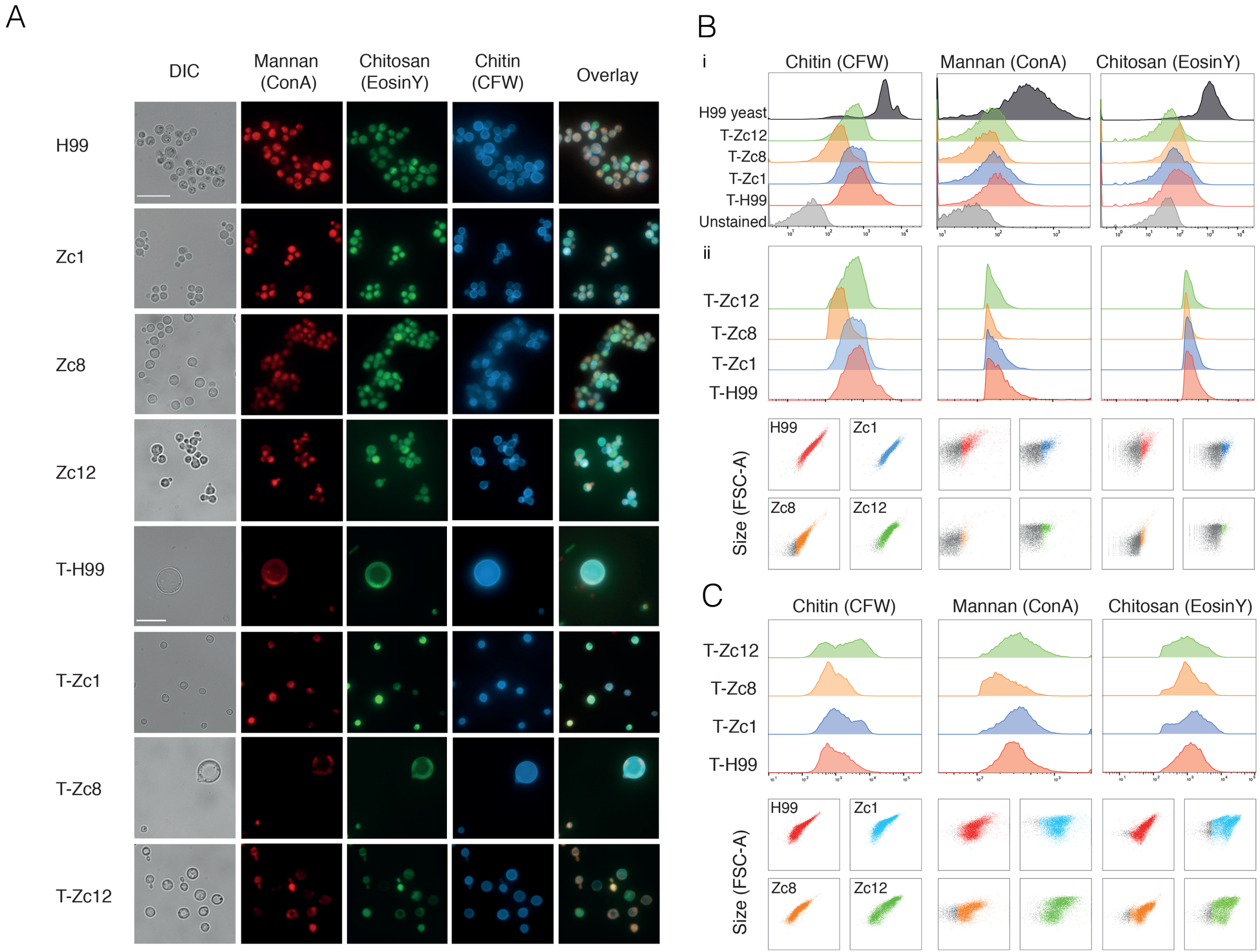
A
DIC
Mannan (ConA)
Chitosan (EosinY)
Chitin (CFW)
Overlay
H99
Zc1
Zc8
Zc12
T-H99
T-Zc1
T-Zc8
T-Zc12
B
i
Chitin (CFW)
Mannan (ConA)
Chitosan (EosinY)
H99 yeast
T-Zc12
T-Zc8
T-Zc1
T-H99
Unstained
ii
T-Zc12
T-Zc8
T-Zc1
T-H99
H99
Zc1
Zc8
Zc12
Size (FSC-A)
C
Chitin (CFW)
Mannan (ConA)
Chitosan (EosinY)
T-Zc12
T-Zc8
T-Zc1
T-H99
H99
Zc1
Zc8
Zc12
Size (FSC-A)